Nano Today 24 (2019) 103–119

Contents lists available at ScienceDirect

Nano Today

journal homepage: www.elsevier.com/locate/nanotoday

Review

Porous carbon nanosheets: Synthetic strategies and electrochemical energy related applications

Yafei He [b], Xiaodong Zhuang [b], Chaojun Lei [a], Lecheng Lei [a], Yang Hou [a,*], Yiyong Mai [b,*], Xinliang Feng [c,*]

[a] Key Laboratory of Biomass Chemical Engineering of Ministry of Education, College of Chemical and Biological Engineering, Zhejiang University, Hangzhou, 310027, China
[b] School of Chemistry and Chemical Engineering, Shanghai Key Laboratory of Electrical Insulation and Thermal Ageing, Shanghai Jiao Tong University, Shanghai, 200240, China
[c] Center for Advancing Electronics Dresden (cfaed) & Department of Chemistry and Food Chemistry, Technische Universität Dresden, Mommsenstrasse 4, Dresden, 01062, Germany

ARTICLE INFO

Article history:
Received 10 October 2018
Received in revised form
25 November 2018
Accepted 24 December 2018
Available online 1 January 2019

Keywords:
Porous carbon nanosheet
Two-dimensional
Precursor
Template
Electrochemical energy device

ABSTRACT

Development of two-dimensional (2D) porous carbon nanosheets (PCNs) with an interlinked hierarchical porous structure has attracted great attention due to their synergetic features combining both 2D materials and porous architectures. In recent years, rapid development of synthetic methods for the fabrication of PCNs with hierarchical porous structure, high specific surface area, controlled heteroatom doping, and excellent electrical conductivity has shown signifcant potential in energy-related applications. This review article comprehensively summarizes the recent developments in synthetic methods, including the hard template strategy, soft template strategy, and template-free strategy for successful preparation of PCNs. Three representative electrochemical applications of such PCNs materials for lithium ion batteries, supercapacitors, and electrocatalytic oxygen reductions are presented. At the end of this review, the current existing challenges for the controlled synthesis of PCNs with desired properties and future perspectives for developments of new synthesis methods and new electrochemical energy applications are also discussed.

Contents

* Corresponding authors.
E-mail addresses: yhou@zju.edu.cn (Y. Hou), mai@sjtu.edu.cn (Y. Mai), feng@tu-dresden.de (X. Feng).

https://doi.org/10.1016/j.nantod.2018.12.004
1748-0132/

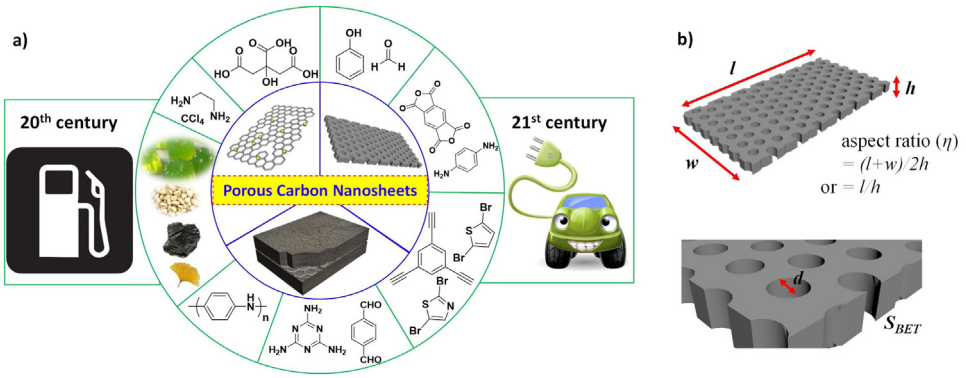

Fig. 1. (a) Summary of the synthesis and energy-related applications of PCNs materials, (b) Typical parameters for PCNs: length (l), width (w), thickness (h) as well as average pore diameter (d) and specific surface area (S_{BET}). Aspect ratio (η) of carbon nanosheets can be estimated from the ratio of width (or length) to height.

Introduction

Entering the 21st century, energy resource shortages and environmental pollution problems caused by heavy consumption of fossil fuels have attracted considerable attention. To overcome these limitations, the developments of high-efficiency energy storage and conversion devices, such as rechargeable batteries [1–3], supercapacitors [4,5], and fuel cells [6–8], etc, has been progressing rapidly in the past decades. A key requirement for the successful implementation of these electrochemical energy-related devices is the development of advanced and cost-effective electroactive materials with unique structural characteristics. Generally, the materials dimensionality can be categorized into zero-dimensional (0D) nanoparticles [9,10], one-dimensional (1D) nanowires/nanotubes [11–16], two-dimensional (2D) nanosheets [17,18], and three-dimensional (3D) networks [19–23]. Different dimensional structures of materials would exhibit different electrochemical performances based on their structural and surface characteristics, as well as their differences in electron/ion transport mechanisms [24–26]. Among 0D, 1D, 2D, and 3D nanostructured materials, 2D nanosheets materials with ultrathin thickness and large lateral size possess unique layered structure, abundant and accessible catalytically active site, as well as unusual physical, chemical, and electronic properties, making them attractive candidates for next-generation electrochemical energy devices [27,28]. The successful preparation of graphene in 2004, which is one-atom-thick and crystalline sp2-carbon sheet, opens a new era of exploration of 2D materials. To date, a considerable number of 2D materials, including black phosphorus, transition metal dichalcogenides, layered double hydroxides, hexagonal boron nitride, metal carbides (MXenes), and porous carbon nanosheets (PCNs), have been successfully synthesized and explored for broad and tremendous applications, especially in the fields of electrochemical energy storage and conversion [29–35], illustrating the great potential of the 2D materials family.

Among the different 2D mateirals for energy related devices, carbon nanosheets [36], especially the PCNs [37], represent one class of the most appealing 2D materials because they can potentially combine the unique properties of 2D carbon materials with the porous features, creating novel physiochemical properties different from those of either common porous carbons or ultrathin nanosheets (Fig. 1a). The PCNs herein refer to those nanoscale-thickness layered porous carbon materials, with the assumption that the thickness of these carbon nanosheets is much smaller than its lateral dimensions (Fig. 1b), including porous heteroatom-doped carbon nanosheets, porous sandwich-like carbon nanosheets composites, porous vertically aligned carbon nanosheets, and porous carbon nanosheets with embedded transition-metal nanoparticles, etc. Although other sheet-type carbon materials, such as holey graphene nanosheets, have also attracted increasing interest due to their wide range of applications, they are beyond the scope of this review (see other papers [38,39]). It is worth mentioning that PCNs have caught the wide attentions [17], up till now, comprehensive reviews that summarize recent progress on their synthetic methods and applications in electrochemical energy device still remain missing.

In this review article, a brief introduction about the advantageous structural features of PCNs materials was firstly provided. The synthetic methods for the fabrication of PCNs by means of hard template strategy, soft template strategy, and template-free strategy, and their representative energy related applications in lithium ion batteries (LIBs), supercapacitors, and electrocatalytic oxygen reduction reactions (ORR), are discussed in detail. A brief summary on the synthetic methods, structural features, and electrochemical performances of these PCNs are provided in Table 1 and Table 2 respectively. The final section gives the perspectives on major challenges and opportunities associated with PCNs materials in energy storage and conversion applications.

Advantages of PCNs materials for energy related applications

In comparison to graphene material, besides the unique physicochemical and electronic properties, the PCNs possess additional structural advantages. For example, 1) the porous feature of PCNs ensures fast mass transportation of the relevant species and efficient electrolyte infiltration to the electrode surfaces, thus providing high electrode-electrolyte interfaces [40,41]; 2) the PCNs offer large specifc surface areas and abundant electrochemically active sites for electrochemical reactions [42–44]; 3) the PCNs enable interconnected hierarchical porous structures, which afford continuous electron transport pathways and shorten ion/mass transport distances through the porous nanosheets [45–47]; 4) the porous structure of PCNs can effectively prevent the irreversible restacking and overlapping that reduce the available active surfaces [48]; 5) the internal free spaces in the PCNs can provide suffcient voids for accommodating volume changes during charge/discharge cycles [49], thus achieving long cycling stability.

Synthesis approaches and electrochemical performances

Hard template method

Hard templating method such as porous silica and layered metal oxide is one of the most popular approaches towards the preparation of nanostructured materials because it can maintain the

Table 1
The summary of specific surface area and electrochemical performance for the PCNs materials prepared by different hard templates.

Sample	Template	Specific surface area ($m^2 g^{-1}$)	Electrochemical performance	Ref.
Mesoporous Co/Fe-N-doped carbon nanosheets	Montmorillonite	239	*Catalyst for ORR:* electron transfer number of 3.95	[57]
Functional nanoporous carbon nanosheets	Zinc hydroxide nanosheets	2402	–	[60]
Fe&Fe_3O_4@PGC nanosheets	NaCl	469	*Electrode material for LIBs:* capacity of 722 mAh g^{-1} at 100 mA g^{-1}	[74]
3D N-doped carbon networks	NaCl and Na_2SiO_3	900	*Electrode material for LIBs:* capacity of 1222 mAh g^{-1} at 100 mA g^{-1}	[77]
Graphene-based porous CN nanosheets	Graphene-based silica nanosheets	542	*Catalyst for ORR:* electron transfer number of 4.0	[90]
Mesoporous PPy/GO nanosheets	Micelle copolymer/graphene	85	*Electrode material for supercapacitors:* capacity of 383 F g^{-1} at 0.001 V s^{-1}	[95]
N-doped carbon nanosheets	Graphene/carbanions hybrids	–	*Catalyst for ORR:* diffusion-limited current density of 5.2 mA cm^{-2}	[100]
Heteroatom-doped (S/N) PCNs	*p*-bromobenzene RGO	681	*Electrode material for supercapacitors:* capacity of 383 F g^{-1} at 0.001 V s^{-1}	[104]
N-enriched 2D porous carbons	Amino-functionalized GO	399	*Electrode material for supercapacitors:* capacity of 424 F g^{-1} at 100 mA g^{-1}	[106]
Vertically aligned porous graphene	$Mg(OH)_2$	1511	*Electrode material for LIBs:* capacity of 1150 mAh g^{-1} at 100 mA g^{-1}	[109]
MoS_2/N-doped porous carbon	MoS_2 nanosheets	850	*Catalyst for ORR:* diffusion-limited current density of 5.4 mA cm^{-2}	[123]

Table 2
The summary of specific surface area and electrochemical performance for the PCNs materials prepared by template-free method from different precursors.

Sample	Precursor	Specific surface area ($m^2 g^{-1}$)	Electrochemical performance	Ref.
2D PCNs	Potassium citrate	2220	*Electrode material for supercapacitors:* high rate capability with 120 F g^{-1} at 0.2 V s^{-1}	[135]
Hierarchical carbon nanosheets	Sodium gluconate	1,890	*Electrode material for supercapacitors:* capacity of 140 F g^{-1} at 150,000 mA g^{-1}	[137]
N-doped carbon nanosheets	EDTA calcium disodium	85	*Catalyst for ORR:* electron transfer number of 3.8	[177]
Carbon superstructures	Polyimide	1375	*Catalyst for ORR:* diffusion-limited current density of 5.5 mA cm^{-2}	[143]
N/S dual-doped PCNs	2D conjugated polymers	1,153	*Catalyst for ORR:* diffusion-limited current density of 5.1 mA cm^{-2}	[148]
Interlinked PCNs	Glucose spheres	2633	*Electrode material for supercapacitors:* Capacity of 184 F g^{-1} at 100,000 mA g^{-1}	[149]
S-doped PCNs	Sulfonic acid ion exchange resin	2005	*Electrode material for supercapacitors:* Capacity of 312 F g^{-1} at 500 mA g^{-1}	[150]
3D carbon networks	Cassava	–	*Polysulfides inhibitor for Li-S batteries:* capacity of 811 mAh g^{-1} after 100 cycles at 0.5 C	[166]
Interconnected carbon nanosheets	Agar	1,750	*Electrode materials for Li-S batteries:* capacity of 1240 mAh g^{-1} at 167 mA g^{-1}	[171]

original morphology during the preparation process [50–52]. It is believed that the deformation of hard templates can be negligible in the synthesis process and the structure of resultant materials enables faithful replication from the templates, resulting in the successful preparation of 2D materials with tunable structure and morphology [53,54]. Because of the remarkable accesibltity of hard templating method to obtain 2D morphology and porous stuctures, this type of method shows the availability in a wide range of materials and sizes, with facility to scale up. To date, three primary types of 2D hard templates have been employed for the fabrication of PCNs materials, including the template with inter-multilayered 2D space, template with single-sided 2D surface from salt grain, and template with other 2D materials surface (Fig. 2).

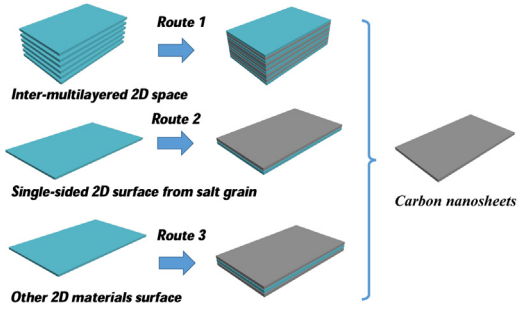

Fig. 2. Three typical hard template routes towards the synthesis of PCNs.

Hard templates with inter-multilayered 2D space

There are various natural and synthetic materials possessing multilayered structures, which can offer desirable 2D confined space. Since the thickness of these layers are usually ultrathin and uniform, they can act as promising hard templates for the preparation of PCNs [55].

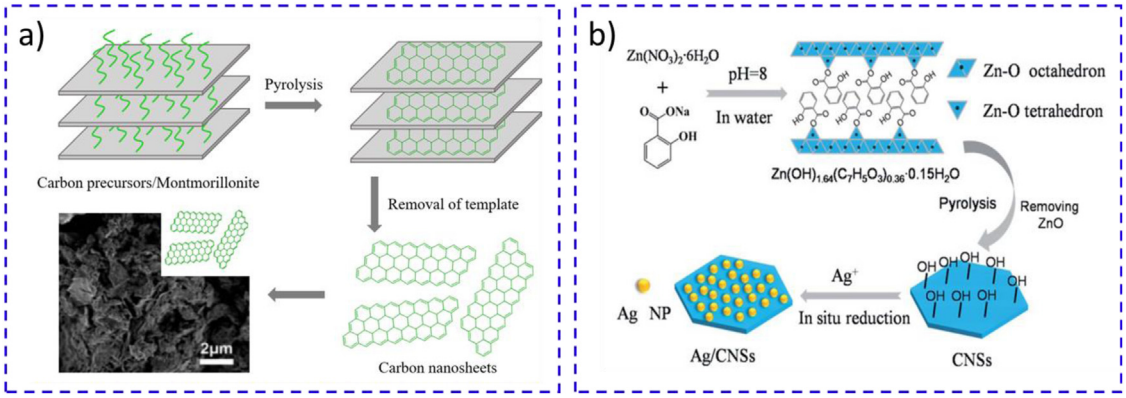

Fig. 3. (a) Schematic illustration of synthetic route to fabricate Co/Fe-*N*-doped carbon nanosheets by using montmorillonite as layered templates (Reproduced with permission [57]. Copyright 2013, American Chemical Society), and (b) Schematic illustration of synthetic route to fabricate hydroxyl-rich nanoporous carbon nanosheets from organic-inorganic multilayer zinc hydroxides nanosheets and their application in the in-situ preparation of well-dispersed Ag NPs. (Reproduced with permission [60]. Copyright 2015, Royal Society of Chemistry).

Montmorillonite possesses a multilayered lamellar structure with open channels, and it has been demonstrated as layered template for producing many kinds of 2D materials via the carbonization of montmorillonite supported long-chain organic molecules or polymers composites [56]. As a typical example, mesoporous Co/Fe-*N*-doped carbon nanosheets with ~100 nm in thickness was prepared via pyrolysis of polyaniline-Fe complex and vitamin B12 (VB12), using the montmorillonite as template (Fig. 3a). The resultant Co/Fe-*N*-doped carbon nanosheets exhibited a catalytic activity for electrochemical ORR in acidic solution, giving an electron transfer number of 3.95, limiting current density of 4.5 mA cm^{-2}, and half-wave potential of 0.79 V [57]. This half-wave potential value of Co/Fe-*N*-doped carbon nanosheets is comparable to that of the best nonprecious metal catalysts in literatures till year 2013, and even only ~0.058 V deviation from commercial Pt/C. The unusual ORR catalytic activity of Co/Fe-*N*-doped carbon nanosheets could be ascribed to the large surface area of 239 $m^2 g^{-1}$, well-defined porous structure, narrow distribution of pores (~4.5 nm), and homogeneous distribution of active sites (metal/N) [57]. In addition to small molecules (e.g. VB12), polymers can also be applied as precursors to produce carbon nanosheets using montmorillonite as template. For example, a facile and environmentally friendly method was established to synthesize PCNs through the carbonization of mixed waste plastics consisting of polystyrene from foam sheets, polyethylene from vessels, and polypropylene from woven bags on the modified montmorillonite, followed by KOH activation. The resultant PCNs was a largely 2D nanoseets with hundred nanometers to several micrometers in lateral size and ~130 nm in thickness. Moreover, the PCNs possessed high pore volume of 3319 $cm^3 g^{-1}$ and large surface area of 2,315 $m^2 g^{-1}$ [58,59].

Apart from montmorillonite, a number of other layered materials such as layered zinc hydroxides [60], mesoporous molecular sieves (Ti-MCM-41) [61], halloysite [62], and zeolite [63] have been also employed as hard templates to produce PCNs. For instance, using multilayer zinc hydroxide nanosheets as a template, functional nanoporous carbon nanosheets with high specific surface area of 2,402 $m^2 g^{-1}$ can be fabricated (Fig. 3b). By pyrolysis of hydrolyzate product of zinc nitrate in alkaline sodium salicylate solution, the salicylate anions of precursors were carbonized into carbon skeletons. After the removal of zinc hydroxide template, the PCNs with a thickness of $\tilde{2}5$ nm and interconnected hollow carbon shells (thickness = 4~6 nm) were generated. The as-prepared PCNs functionalized with hydroxyl groups were capable of *in-situ* loading with Ag nanoparticles (NPs). The final Ag/PCNs composite showed higher catalytic activity (rate constant of 33.82 $s^{-1} g^{-1}$) towards 4-nitrophenol reduction, than those previously reported for carbon supported metal NPs catalysts (e.g. reduced graphene oxide/Ni (RGO/Ni) nanocomposite [60]).

Hard templates with single-sided 2D surface from salt grain

Inorganic salts, such as NaCl, $NaSO_4$, and $Cu(NO_3)_2$, possess typical crystal structures with regular grain shapes, and the outside surface of such salt grain can afford desirable substrate as structural-templates [64,65]. Especially, some inorganic salts with excellent thermostability can be directly used as templates for the carbonization of organic precursors, and their crystal structures are preserved after high-temperature reaction. Since the removal of salt template is facile and safe, the salt template method that is a typical process of dissolution-recrystallization-pyrolysis, has been extensively explored for the preparation of PCNs [66–71]. For instance, ferrite/carbon hybrid nanosheets were prepared via the carbonization of ferric-oleate precursor using Na_2SO_4 salt as a template (Fig. 4). Specifcally, mixing ferric-oleate with Na_2SO_4 resulted in the ferric-oleate complex coated uniformly on the surface of Na_2SO_4 particles. Subsequent thermal treatment of the above-mentioned mixture at 600 °C under N_2 atmosphere, followed by water washing that produced the ferrite/carbon hybrid nanosheets containing uniformly distributed ferrite NPs. The sizes of ferrite NPs could be controlled by the heating rates during carbonization process; higher heating rates resulted in smaller particle sizes. The achieved 2D ferrite/carbon hybrid nanosheets was employed as electrode material in LIBs, affording a 68.7% capacity retention at 5000 mA g^{-1} and specific capacity of 660 mAh g^{-1} at 100 mA g^{-1} [72].

Considering that NaCl is more easily precipitated than metal precursors during recrystallization, it has been extensively explored as an important salt-template to fabricate PCNs based hybrids [73]. As a typical example (Fig. 5a), a facile, scalable synthesis strategy was developed to prepare PCNs by using NaCl as template, iron nitrate as metal precursor, and glucose as carbon precursor. After pyrolysis and subsequent washing with H_2O, the PCNs with Fe and Fe_3O_4 NPs embedded in the carbon frameworks (Fe&Fe_3O_4@PCNs) were obtained. The resultant Fe&Fe_3O_4@PCNs had a nanosheets morphology with ~50 nm in thickness and 1–10 μm in lateral size. After etching the Fe and Fe_3O_4 NPs, the PCNs were achieved which showed abundant porous structure with high specific surface area of ~469 $m^2 g^{-1}$ and total pore volume of ~0.83 $cm^3 g^{-1}$. Consequently, a high reversible capacity of 722 mAh g^{-1} was obtained after 100 cycles at 100 mA g^{-1} for the resultant PCNs in LIBs, which was much higher than theoretical specific capacity of graphite (~372 mAh g^{-1}) [74]. Similarly, porous FeS/C nanosheets were successfully prepared by using NaCl-

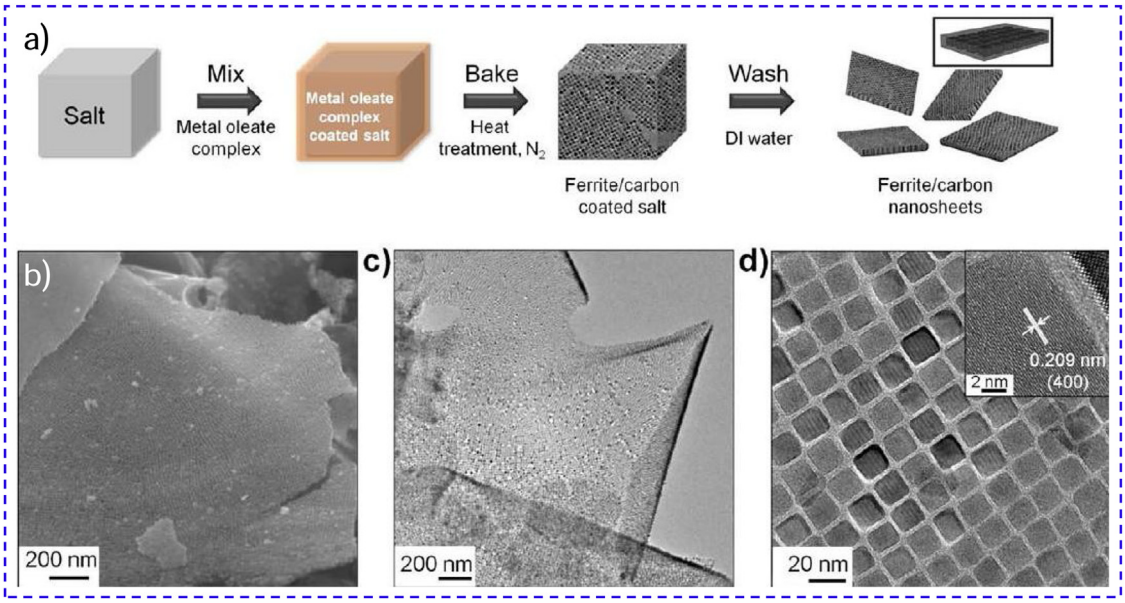

Fig. 4. (a) Schematic illustration of synthetic route to fabricate ferrite/carbon nanosheets by salt-template approach, (b) Field-emission scanning electron microscopy (FESEM) image, and (c, d) Transmission electron microscopy (TEM) images of iron-oxide/carbon nanosheets. The inset shows high resolution TEM (HRTEM) image of ferrite/carbon nanosheets, demonstrating the uniform dispersion of ferrite NPs embedded into carbon nanosheets. (Reproduced with permission [72]. Copyright 2012, American Chemical Society).

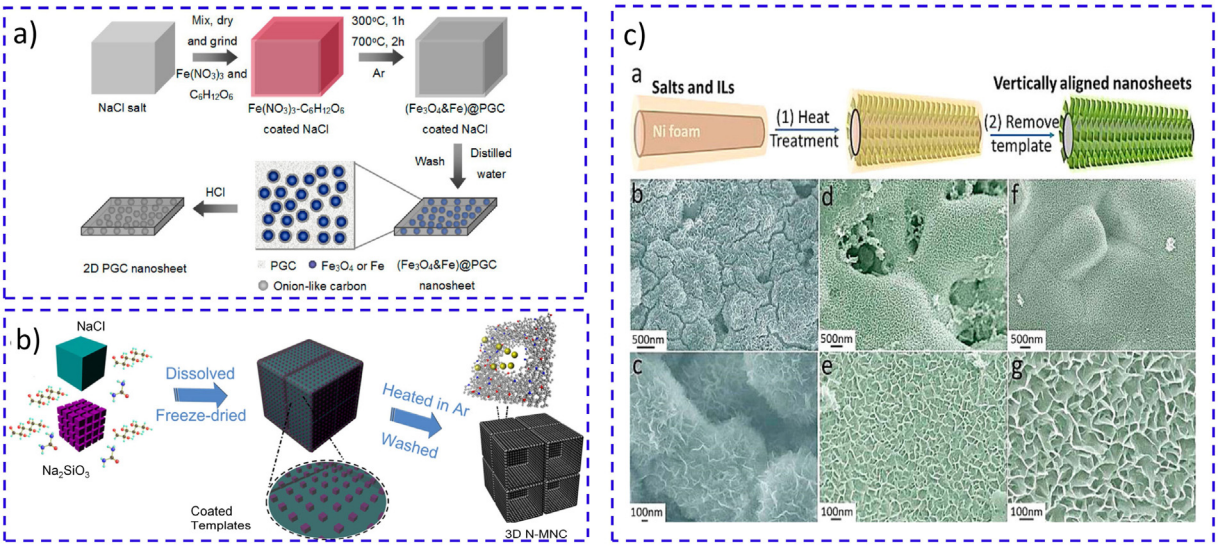

Fig. 5. (a) Schematic illustration of synthetic route to fabricate 2D graphitic PCNs using NaCl as template (Reproduced with permission [74]. Copyright 2013, American Chemical Society), and (b) Schematic illustration of synthetic route to 3D N-doped carbon networks constructed by mesoporous nanosheets using Na_2SiO_3 and NaCl as dual salt-templates (Reproduced with permission [77]. Copyright 2016, American Chemical Society), and (c) Schematic illustration of salt-templating process to fabricate vertically aligned functional carbon nanosheets on Ni foam and their typical FESEM images. (Reproduced with permission [78]. Copyright 2015, American Chemical Society).

template method, which delivered a remarkable electrochemical performance with a specifc capacity ~703 mAh g^{-1} at current density of 1000 mA g^{-1} after 150 cycles, and there was about ~532 mAh g^{-1} even at current density of 5000 mA g^{-1}, which is among the best records for FeS-based anode materials in LIBs [75].

On the other hand, the salt-tempate strategy is also applicable to the construction of diverse 3D carbon frameworks that consist of 2D carbon nanosheets through the combination of different salt templates with different grain sizes [76]. For example, 3D carbon networks composed of N-doped carbon nanosheets were fabricated via a one-pot strategy with Na_2SiO_3 and NaCl as dual templates (Fig. 5b). The Na_2SiO_3 with smaller particle size was grown on the NaCl with particle size of 1–2 μm to establish 3D hierarchical templates. By dissolving the precursors of glucose and urea into salt solution and subsequent freeze-drying treatments, 3D glucose-urea complex was uniformly coated onto the salt templates. After high-temperature pyrolysis of the mixed precursors at 700 °C and subsequent removal of template by water washing treatment, N-doped mesoporous carbon nanosheets with interconnected 3D frameworks was obtained. The resulting nanosheets had a thickness of less than 5 nm with closely packed mesopores of 5–7 nm. The achieved 3D N-doped carbon networks exhibited hierarchical macro/mesoporous structures and specific surface area of 900 $m^2 g^{-1}$. Moreover, the mesoporous structure of the 3D networks could be adjusted by simply changing the Na_2SiO_3/NaCl weight ratio, and the N-doping content could be tuned by tailoring the ratio

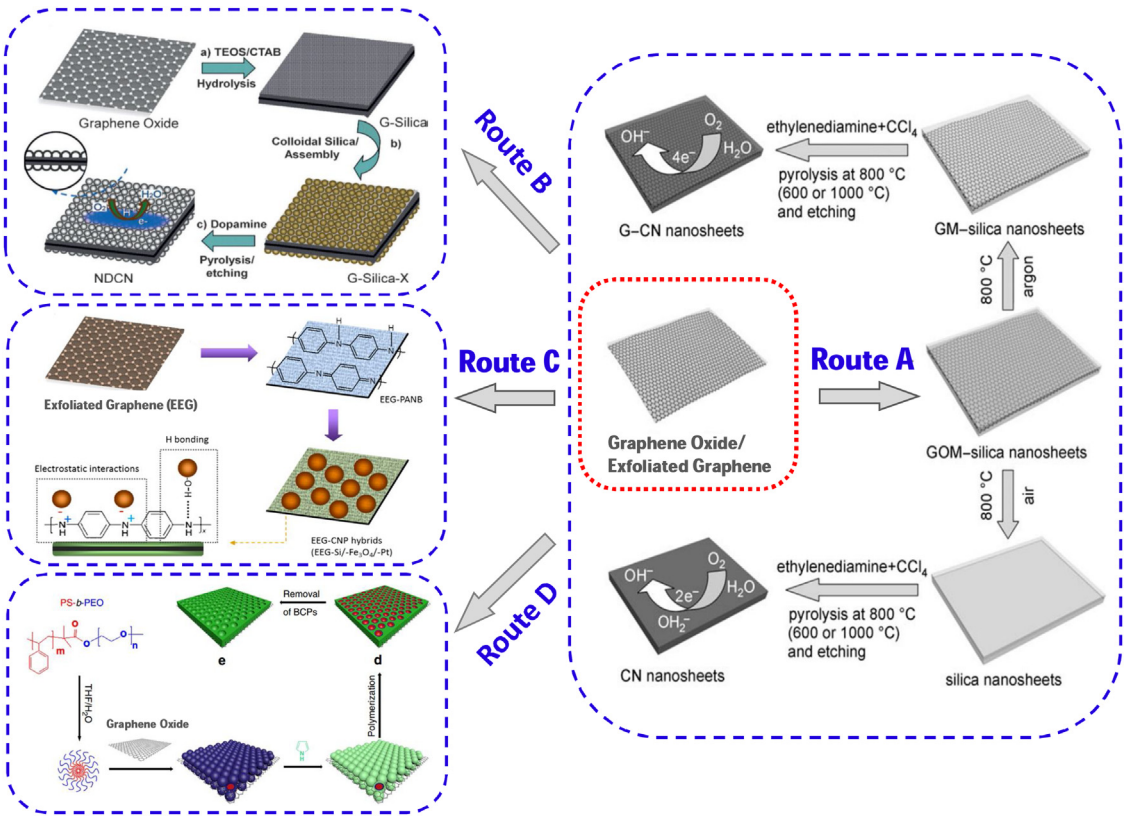

Fig. 6. Schematic illustration of synthetic route to fabricate G-CN and CN nanosheets using mesoporous GM-silica nanosheets and mesoporous silica nanosheets as sandwich-like templates (Route A) (Reproduced with permission [90]. Copyright 2011, Wiley-VCH), NDCN with uniform and tunable mesopores (Route B) via the templating of graphene/silica nanosheets (Reproduced with permission [91]. Copyright 2011, Wiley-VCH), novel 2D hybrids with various colloidal NPs including Si, Fe_3O_4, and Pt NPs coupled onto EEG nanosheets via polyaniline in the emeraldine base form (Route C) (Reproduced with permission [92]. Copyright 2015, American Chemical Society), and mPPy nanosheets templated by closely packed diblock copolymer of PS-b-PEO micelles attached on GO (Route D). (Reproduced with permission [95]. Copyright 2015, Macmillan Publishers Limited).

between nitrogen and carbon sources. Benefiting from the hierarchical structure and N dopant, the obtained 3D networks showed outstanding specific capacity of 1222 mAh g^{-1} at 100 mA g^{-1}, and remarkable cycling stability with retained capacity of 604 mAh g^{-1} after 600 cycles at high current density of 2000 mA g^{-1} [77]. Such a high specific capacity of 1222 mAh g^{-1} at 100 mA g^{-1} is comparable to those of the best carbon-based anodes in literatures till year 2016. In another example, a series of vertically aligned carbon nanosheets hybrids (MoC@CNS, WC@CNS, TaC@CNS, and NbC@CNS) grown on Ni foam were fabricated by applying the similar dual salt-templates strategy (Fig. 5c). Vertically aligned carbon nanosheets with 100–200 nm in lateral size and ~5 nm in thickness were fully covered on the Ni foam, along with metal-carbide NPs (~5 nm in diameter) embedded in carbon matrix. The resultant hybrids delivered an average specific capacity of 1010 mAh g^{-1} at 200 mA g^{-1} [78], which is approaching that of aforementioned 3D N-doped carbon networks (1222 mAh g^{-1}).

Hard templates with other 2D materials surface

Graphene-based template. In the past few years, graphene materials have been widely explored for electrochemical energy related applications due to its unique properties, such as high electrical conductivity, high specifc surface area, and good thermal/mechanical stability [79–82]. By using graphene as hard template, massive efforts and progresses have been devoted to prepare a variety of new 2D carbon-based materials with diverse nanostructures [83,84]. Graphene oxide (GO), a popular graphene derivative with abundant oxygen-containing functional groups, is an alternative template for the construction of 2D materials [85]. In this section, we focus on the design and fabrication of graphene-based hybrids by control of the interactions, including non-covalent interaction and covalent interaction, between graphene-based templates and precursors.

Noncovalent interaction of graphene with precursors. Graphene or GO can act as the template for the synthesis of carbon materials with unique 2D nanostructures [83]. Further formation of micro- and/or meso-porous structures within the obtained 2D nanocarbons may facilitate ion and electron transport process as well as increase the specific surface area, thus resulting in the enhancement of their electrochemical properties [86–88]. In view of this, different types of NPs, including SiO_2 NPs, Fe_3O_4 NPs, Pt NPs, and block copolymer micelles have been used as pore-creating templates (Fig. 6) [89].

For instance, a novel GO-based silica (GOM-silica) nanosheets with a sandwich structure was prepared by hydrolysis of TEOS/GO hybrid precursor in the presence of cetyltrimethyl ammonium bromide surfactant. The GOM-silica nanosheets was reduced into mesoporous graphene-based silica (GM-silica) nanosheets by annealing treatment under Ar atmosphere, while the GOM-silica nanosheets was transformed into mesoporous silica nanosheets by annealing treatment under air atmosphere. The ethylenediamine with carbon tetrachloride was subsequently impregnated into the GM-silica and silica nanosheets templates. After further pyrolysis and acid etching treatment, porous carbon nitride (G-CN)/graphene nanosheets and porous CN nanosheets were produced, respectively (Fig. 6). These nanosheets with nanometer-scale thickness possessed prominent features, including ultrahigh N-contents of up to 10% and high surface area of 542 m^2 g^{-1} with hierarchical porous

structure. As metal-free ORR electrocatalysts, the G-CN produced a kinetic current density of 7.3 mA cm^{-2}, electron transfer number of 4.0, and long durability with a slight loss of specific catalytic activity under continuous catalysis (30,000 s) at -0.25 V [90]. This value of 7.3 mA cm^{-2} for the G-CN was much larger than that of commercial Pt/C (5.4 mA cm^{-2}) in alkaline condition. A similar approach was used to fabricate N-doped carbon nanosheets (NDCN) with tunable pore architecture by employing mesoporous silica/graphene hybrid nanosheets and polydopamine as template and carbon precursor (Fig. 6). The porosity structure was controlled by adjusting the pore size of mesoporous silica NPs. The obtained NDCN (22 nm pore diameter) could be an effcient catalyst for ORR [91], showing more positive onset potential of -0.01 V as compared with the Pt/C (-0.02 V) in alkaline solution. The diffusion-limited current density of NDCN was 5.45 mA cm^{-2} that is approaching to the value of Pt/C (5.78 mA cm^{-2}), which marked the most efficient metal-free carbon-based ORR catalysts till year 2014. In addition to silica NPs, other types of NPs could be also applied as functional materials by adsorption on graphene surfaces. Fig. 6 displays a typical bottom-up approach for the fabrication of other 2D hybrids. For instance, during the reaction process, emeraldine base-form polyaniline (PANI) adsorbed onto the surface of electrochemically exfoliated graphene (EEG) by π-π interactions, while various colloidal Pt, Fe_3O_4, or Si NPs were further coupled with the exposed imine/amine reactive sites of PANI/EEG. As electrode material in LIBs, the obtained EEG-Si electrode showed high initial specifc capacity of 2357 mA h g^{-1} at 105 mA g^{-1} and 86% capacitance retention at 1000 mA g^{-1} after 100 cycles [92], which exceeds that of the reduced GO-Si anode material (1709 mA h g^{-1}).

Block copolymer micelles that can be sacrificed by solvent dissolution or pyrolysis are one of desirable candidates serving as pore-creating templates to construct porous materials [93,94], as the dimension of micelle cores is readily tunable by changing the length of hydrophobic blocks in the micelle-forming copolymers. As a typical example, a solution-based self-assembly protocol was developed for the preparation of mesoporous PPy (mPPy) or PANI nanosheets grown on different kinds of 2D materials (e.g., EEG, GO, MoS_2, and titania nanosheets) by using polystyrene-b-poly(ethylene oxide) (PS-b-PEO) micelles as template (Fig. 6). By varying PS block lengths, the mPPy@GO nanosheets with thickness of 35–45 nm, specific surface area of up to 85 m^2 g^{-1}, and pore size of 5–20 nm could be easily prepared. As an electrode material, the resultant mPPy@GO nanosheets with mesopore size of 5.8 nm delivered a larger specific capacitance of 383 F g^{-1} at scan rate of 0.001 V s^{-1}, than that of the mPPy@GO nanosheets with larger mesopore sizes of 19.3 nm (302 F g^{-1}) or 13.2 nm (368 F g^{-1}), and even better than those reported for other PPy/graphene based hybrid materials till year 2015 [95].

Covalent interaction of graphene with precursors. Except for the above noncovalent interaction coupled on graphene-based materials, the covalent interaction with graphene-based templates is an alternative pathway to build up 2D porous polymer/graphene composites [96]. The unique structural features of graphene confined within polymer networks can offer numerous opportunities for the template-directed synthesis of porous polymers with controlled morphologies [97]. Moreover, as-prepared 2D porous polymer composites are desirable precursors for further fabrication of PCNs by subsequent thermal treatment [98,99]. In this subsection, few typical PCNs derived from 2D porous polymer coupled graphene-based composite materials are discussed.

For example, hierarchical PCNs were obtained by pyrolysis of 2D porous polymers that were synthesized via direct growth of linear polymers containing N-containing acrylonitrile monomer on the graphene-based templates (Fig. 7a). The resultant polyacrylonitrile-grafted RGO with thickness of ~7 nm was carbonized at elevated temperatures to afford N-doped carbon nanosheets (NCNSs). The obtained NCNSs showed electrocatalytic performance for ORR with kinetic-limited current density of 21.1 mA cm^{-2} and diffusion-limited current density of 5.2 mA cm^{-2} [100]. The kinetic limiting current density value of NCNSs (21.1 mA cm^{-2}) was much larger than that of the aforementioned G—CN (7.3 mA cm^{-2}) and even commercial Pt/C (18.5 mA cm^{-2}). In another case (Fig. 7b), trithiocarbonate-based chain-transfer agent (CTA) was used to functionalize the GO, resulting in the formation of 2D CTA/GO, which could further initiate the reversible addition fragmentation chain transfer polymerization of 1,4-divinylbenzene and 4-vinylbenzyl chloride to produce poly(vinylbenzyl chloride-co-divinylbenzene) decorated GO nanosheets. After hyper-cross-linking of benzyl chloride groups by $FeCl_3$-promoted Friedel-Crafts reaction, 2D microporous polymers (GHCPs)-graphene hybrid with a sandwiched structure was successfully synthesized with a upscalable quantity of ~100 g. The specific surface area of 1224 m^2 g^{-1} for GHCPs was much larger than that of unadorned hyper-cross-linked microporous polymers synthesized without using graphene template (600 m^2 g^{-1}). After carbonization of GHCPs at 900 °C, the resultant 2D PCNs with specific surface area of 871 m^2 g^{-1} achieved a specific capacitance of 144 F g^{-1} at 500 mA g^{-1} when applied as electrode material in supercapacitors [101].

Conjugated microporous polymers (CMPs) with large surface area have been rapidly developed due to the following advantages of availability of various commercial functional monomers, facile synthetic approach, and exceptional electronic and optoelectronic properties [102,103]. Several moden chemical reactions have been applied for the synthesis of diverse 2D CMPs by using surface-functionalized graphene as structure-directing template. The resulting 2D CMPs was then used as precursors for the preparation of PCNs. For instance, a graphene-inspired synthesis route was developed for large-scale synthesis of 2D sandwich-like CMPs with high surface areas of 888 m^2 g^{-1} and large aspect ratios (several micrometers in lateral size and 40 nm in thickness) (Fig. 7c). In this strategy, thiazole-, thiophene-, or pyridine-based monomers were polymerized with the 1,3,5-triethynylbenzene functionalized graphene by a facile metal-catalyzed Sonogashira-Hagihara type cross-coupling reaction. The obtained 2D polymers were employed as precursors for the fabrication of heteroatom-doped (S/N) PCNs by carbonization treatment at 800 °C. The achieved 2D S/N-doped PCNs exhibited electrochemical performance with a higher diffusion-limited current density of up to 4.0 mA cm^{-2} for ORR [104], as compared with the Co/Fe-*N*-doped carbon nanosheets (4.5 mA cm^{-2}) and Pt/C catalyst (BASF, ~5.5 mA cm^{-2}). Also, the higher electrocatalytic stability of 2D S/N-doped PCNs for ORR was achieved compared with that of Pt/C catalyst. Along this line, *p/n* heterostructures consisting *p*-bromobenzene functionalized graphene (acting as acceptors) and CMPs (acting as donors) were obtained by the above strategy (Fig. 7d). The typical *p/n* 2D heterostructure was successfully prepared via direct polymerization of 1,3,5-triethynylbenzene and halogenated BODIPY (2,6-diiodo-1,3,5,7-tetramethyl-8-phenyl-4,4-difluoroboradiazaindacene) on graphene surfaces. After post-treatment of pyrolysis, the resulting 2D B/N co-doped porous carbons showed an ORR activity with diffusion-limited current density of 6.0 mA cm^{-2} and half-wave potential of 0.71 V [25]. Although the half-wave potential of abovemetioned Co/Fe-*N*-doped carbon nanosheets (0.79 V) was slightly more positive than that of 2D B/N co-doped porous carbons, the limiting current density of 6.0 mA cm^{-2} for 2D B/N co-doped porous carbons was much larger than that of Co/Fe-*N*-doped carbon nanosheets (4.5 mA cm^{-2}).

Apart from CMPs, other types of porous polymers with 2D nanostructures were also synthesized and then transformed into PCNs. For instance, B/N co-doped PCNs with thickness of ~20 nm and high B/N doping amounts (5.3% N and 5.4% B) was synthesized

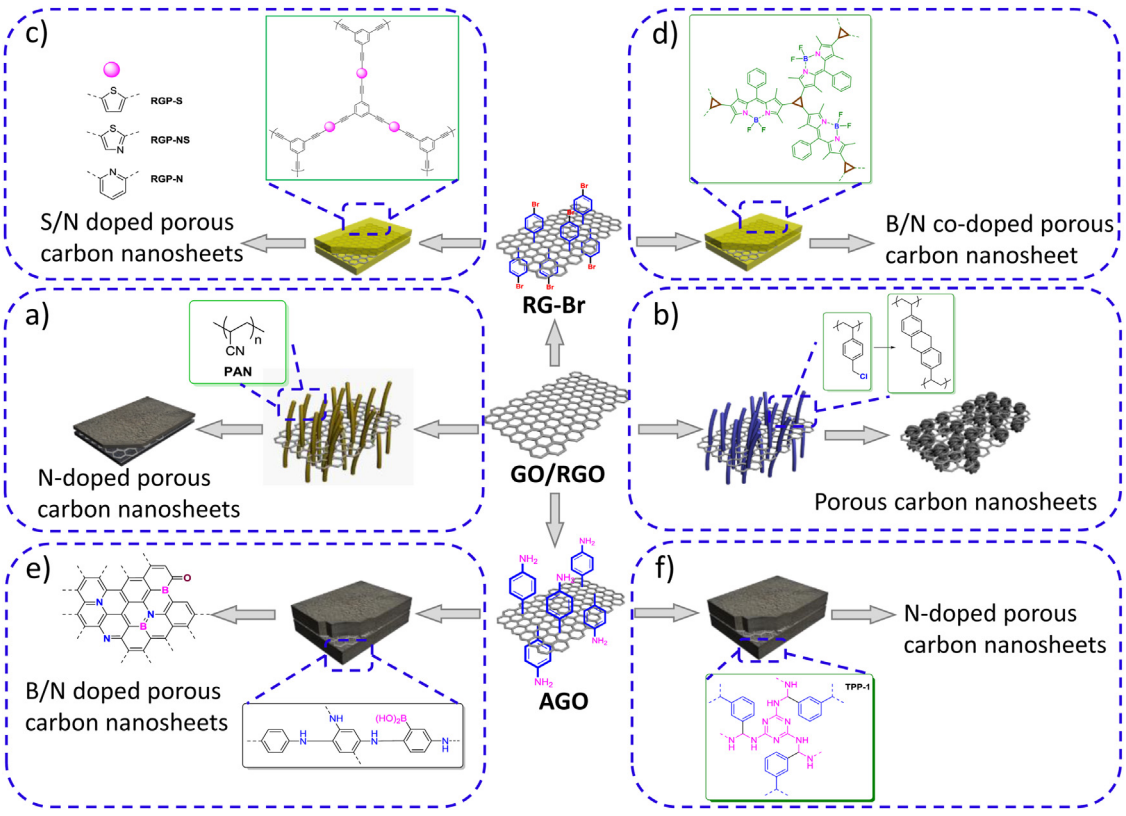

Fig. 7. Schematic illustration of the strategy for (a) polyacrylonitrile-grafted RGO nanosheets by anionic polymerization and corresponding NCNSs (Reproduced with permission [100]. Copyright 2014, Royal Society of Chemistry), (b) 2D graphene-based sandwich-type GHCPs obtained by reversible addition-fragmentation chain transfer emulsion polymerization (Reproduced with permission [101]. Copyright 2015, Royal Society of Chemistry), (c, d) 2D core-shell type CMPs via Sonogashira-Hagihara coupling reaction using *p*-bromobenzene functionalized graphene as template and corresponding S/N doped carbon nanosheets and B/N doped carbon nanosheets (Reproduced with permission [25,104]. Copyright 2013 and 2015, Wiley-VCH), (e) GO-based PNAI nanosheets functionalized with boronic acid and B/N co-doped PCNs prepared by amino-functionalized GO as template (Reproduced with permission [105]. Copyright 2014, Royal Society of Chemistry), and (f) Schiff-base-type 2D TPP nanosheets and N-doped carbon nanosheets via amino-functionalized GO template. (Reproduced with permission [106]. Copyright 2014, Wiley-VCH).

by pyrolysis of GO/PANI nanosheets-boronic acid hybrid precursor at 1000 °C [105]. The obtained B/N co-doped PCNs reached a slightly higher diffusion-limited current density of 4.5 mA cm^{-2} under alkaline conditions (Fig. 7e), than that of 2D S/N-doped PCNs (4.0 mA cm^{-2}). As another example, an effective amino-functionalized GO template strategy was developed for the fabrication of Schiff-base type porous polymer (TPP) nanosheets based on monomers of melamine and aromatic dialdehydes (Fig. 7f). The thickness of TPP nanosheets was tuned from 17 to 290 nm by changing monomer/amino-functionalized GO weight ratio (80/20∼95/5). The resulant TPP nanosheets with ultrahigh N-doping amount of up to 43.9 wt.% were applied as precursors to prepare N-enriched 2D porous carbons (TPC). Benefiting from high surface area (399 $m^2\ g^{-1}$) and high N-doping content (up to 12.3%), the achieved TPC showed a higher specific capacitance of 424 F g^{-1} at 100 mA g^{-1} [106], than that of the carbonized porous carbons derived from TPP without using graphene template, and the abovemetioned mPPy@GO nanosheets.

D materials-based template beyond graphene. In addition to graphene-based materials, a variety of other 2D materials (such as SiO_2 nanosheets, 2D metallic oxide or metal hydroxide, MgAl-layered double oxides (LDO) nanosheets, *g*-C_3N_4, 2D transition-metal dichalcogenides (TMDs), etc.) with unique physical and chemical properties have been also used as hard templates for fabrictaion of 2D carbon-based materials.

For instance, using coal tar pitch as the carbon precursor and SiO_2 nanosheets as the structure-directing template, mesoporous carbon sheet-like framework (MCSF) was synthesized by carbonization of the mixture of SiO_2 nanosheets with ordered mesopores of 2 nm and coal tar pitch at 900 °C. After that, the SiO_2 nanosheets template was dissolved by acid etching treatment. The resultant MCSF was composed of nanosheets structure with pore sizes of 2–15 nm and specific surface area of 583 $m^2\ g^{-1}$. When applied as electrode material in supercapacitors, the MCSF material exhibited specific capacitance of 264 F g^{-1} when the scan rate was 0.005 V s^{-1}, 74% retention ratio at 1 V s^{-1}, and long-term cycling stability (91% of initial capacitance was retained after 5000 cycles) [107]. This specific capacitance value of 264 F g^{-1} for MCSF is almost twice that of carbonized GHCPs (144 F g^{-1}).

2D metallic oxide or metal hydroxide nanosheets such as MgO nanosheets, $Mg(OH)_2$ nansheets, and $Co(OH)_2$ nanosheets have been also utilized as hard templates to prepare 2D carbon-based materials. For example, a large-scale production of pillared PCN (PPCN) was achieved by applying porous MgO nanosheets as the template (Fig. 8a). Self-supporting layered PPCN with mesopores sizes of 6–8 nm was formed through the carbonization of coal tar pitch accompanied with deposition of carbon layers on the surface of porous MgO nanosheets. In this strategy, the specific surface area of MgO template could be controlled by different boiling times, leading to the final PPCN materials with different nanostructures. The well-developed conductive networks and interconnected hierarchical porosities of PPCN contributed synergistically to a comparable electrochemical performance for supercapacitors with specific capacity of 289 F g^{-1} at 0.002 V s^{-1} and capacity retention ratio of 76% from 50 to 1 V s^{-1} [108], to that of the MCSF electrode (264 F g^{-1}). Except for the above metallic oxide nanosheets, metal hydroxide nanosheets have been proved

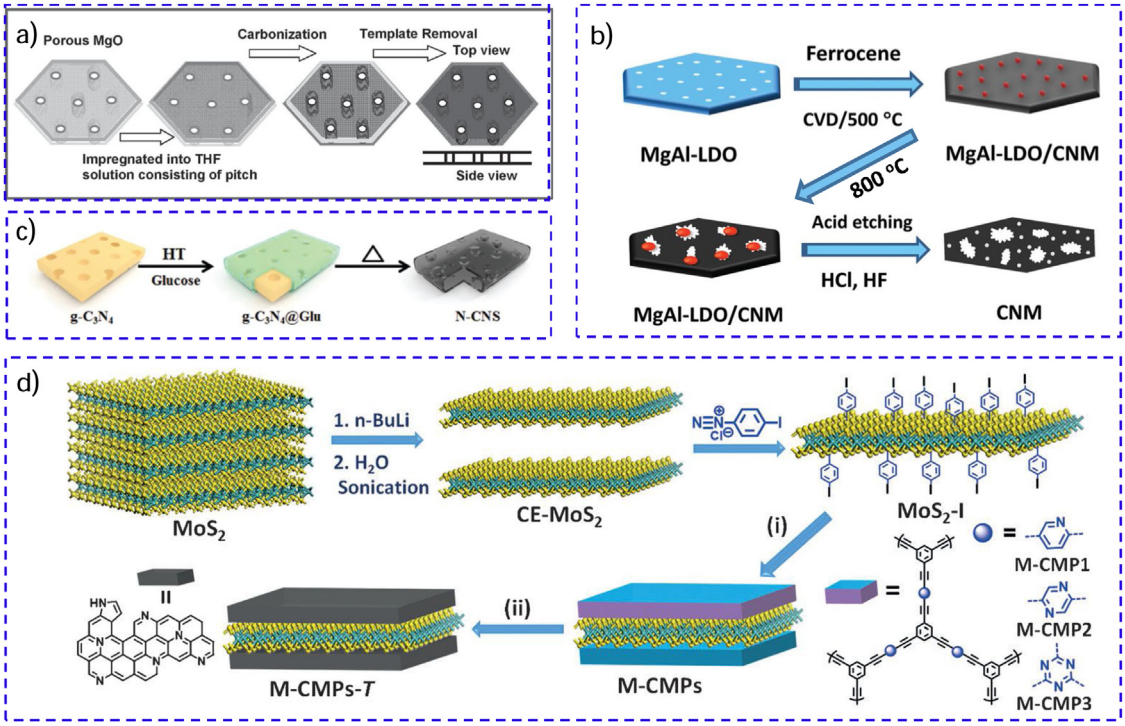

Fig. 8. Schematic illustration of preparation steps for (a) pillared PCNs using porous MgO nanosheets as template (Reproduced with permission [108]. Copyright 2012, Wiley-VCH), (b) CNM using MgAl-LDO as template (Reproduced with permission [111]. Copyright 2015, Wiley-VCH), (c) N-doped PCNs templated from 2D g-C_3N_4 (Reproduced with permission [114]. Copyright 2016, Wiley-VCH), and (d) 2D M-CMPs-T templated from MoS_2/4-iodophenyl diazonium hybrids. (Reproduced with permission [123]. Copyright 2016, Wiley-VCH).

to be good candidates as 2D templates. Briefly, $Mg(OH)_2$-template method was reported to prepare vertically aligned porous graphene (HPCMs) in stick-like morphology with hierarchical porous structure and specific surface area of 1511 $m^2 g^{-1}$ [109]. Hollow Co_3O_4 NPs embedded in carbon nanosheets (thickness of several ten nanometers) grown on Ni foam could be successfully prepared using $Co(OH)_2$ nanosheets array template [110].

Aside from metallic oxide and metal hydroxide nanosheets, MgAl-layered double oxides (MgAl-LDO) nanosheets have been proven to be a kind of emerging templates for the preparation of carbon nanosheets. For example, by using MgAl-LDO as the structural-directing template and the ferrocene as carbon precursor, a combined chemical vapor deposition (CVD) and subsequent thermal annealing method was developed to fabricate the hexagonal thin-sheet carbon nanomesh (CNM) (Fig. 8b). The resultant CNM possessed hollow interior with edge thickness of 50–90 nm, and hierarchical porous structures (micropores of 1–2 nm and mesopores of 2–6 nm). The density and pore size of the mesopores inside CNM could be readily controlled through CVD and annealing time. Acting as electrode material in supercapacitors, the resultant CNM60-90 achieved a specific capacitance of 182 F g^{-1} at 250 mA g^{-1}, with excellent cycling stability of 97% capacitance retention after 20,000 cycles at 3000 mA g^{-1} [111].

Recently, g-C_3N_4 as an important kind of conjugated organic semiconductor comprising of sp2 hybridized N and C atoms with ultrahigh N-content of 57.1 at.% [112], has been widely investigated as both nitrogen source and 2D template to fabricate N-doped PCNs [113]. Typically, glucose was loaed onto both sides of g-C_3N_4 nanosheets via hydrothermal treatment to form g-C_3N_4@glucose composites (Fig. 8c). By pyrolysis at 900 °C, the g-C_3N_4@glucose was converted into N-doped PCNs, which had hierarchical micro/mesoporous structures, large surface area of 1077 $m^2 g^{-1}$, and high N-doping amount ~11.6 at.%. Benefiting from these merits, the N-doped PCNs exhibited excellent ORR performance in different control examples, realizing half-wave potential of 0.75 V and diffusion-limited current density of 5.79 mA cm^{-2} in basic electrolyte [114], which was well comparable to the state-of-art Pt/C catalyst (0.75 V and 5.72 mA cm^{-2}), and even superior to that of those reported metal-free electrocatalysts till year 2016.

Featuring unique 2D structure and ultrathin thickness, 2D TMDs nanosheets, such as MoS_2, WS_2, and $MoSe_2$, have recently shown significant potential applications in energy storage and electrocatalysis [115–122]. Hybridizing MoS_2 nanosheets with porous carbon materials, to construct 2D carbon-based composites is an effective strategy to retain their individual advantages, including excellent electrochemical property, high electrical conductivity, and large surface area [120]. In this respect, 2D MoS_2-coupled microporous polymers (M-CMPs) with a sandwiched structure and its derivatives of 2D MoS_2/N-doped porous carbon (M-CMPs-T) composites (T represents the pyrolysis temperature) were recently synthesized (Fig. 8d). In this strategy, chemically exfoliated MoS_2 nanosheets was decorated with 4-iodophenyl diazonium, followed by growth of CMPs through Sonogashira-Hagihara reaction to obtain triazine-, pyrazine-, and pyridine-containing polymers (M-CMPs). After pyrolysis treatment, the resultant M-CMPs-T material with specific surface area of 850 $m^2 g^{-1}$ delivered a high diffusion-limited current density of 5.4 mA cm^{-2} [123], which acted as electrocatalyst for ORR.

Soft template method

Self-assembly of amphiphilic small molecules or block copolymers (BCPs) can form lamellar structures under appropriate conditions, in which the hydrophobic alkyl chains or blocks of the amphiphilic molecules constructed a planar bilayer that is sandwiched by two hydrophilic shells consisting of the hydrophilic segments of the amphiphiles [124–126]. These lamellaes are ideal

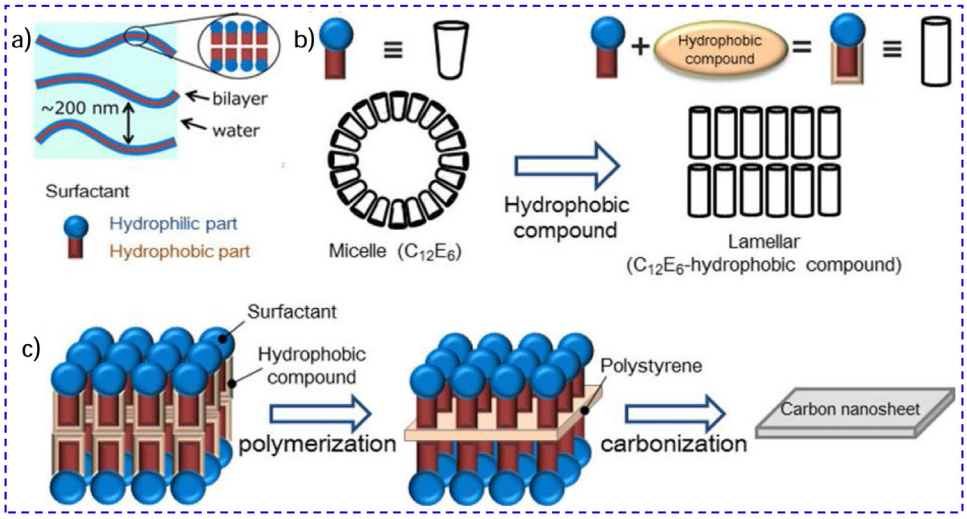

Fig. 9. Schematic illustration of the synthesis routes by using hyperswollen lyotropic lamellar structures formed by amphiphilic bilayers consisted of nonionic polyethylene glycol monoalkyl ether as soft template to prepare PCNs. (Reproduced with permission [129]. Copyright 2016, American Chemical Society).

soft templates for the preparation of PCNs. The unique lamellar structure shows distinct advantages in control of the average thickness and pores structure of the resultant 2D materials, through adjusting the length of hydrophobic segments of lipid molecules or BCPs. Moreover, it is convenient and high-effcient to construct the lamellaes under the suitable condtions as well as to remove the templates by nontoxic or noncorrosive solvents, which is economic and eco-friendly [127]. When using such a strategy, carbon precursors can be adsorbed on the surface of soft templates by hydrogen bondings or electrostatic interactions, which afford more factors to control pore structures of the resultant materials via varying the nature of solvent, temperature, pH, additives, etc [128]. Therefore, soft template method generally appears more flexible in morphological control than hard template approach. Nevertheless, the stability of soft template is worse than hard template, which needs to be further improved. This section introduces several typical examples of constructing PCNs by employing the lamellaes formed via amphiphilic small molecules and BCPs as the 2D templates, respectively.

Amphiphilic small molecules

Fig. 9 presents the preparation of ultrathin carbon nanosheets using hyperswollen lyotropic lamellae as soft template. The hyperswollen lyotropic lamellaer were formed by the amphiphilic bilayers, which consisted of hydrophilic and hydrophobic segments of nonionic polyethylene glycol monoalkyl ether (C_mE_n: m and n denote the number of carbon atoms in alkyl chain and number of repeating unit of ethylene glycol, respectively). The volume ratio of the hydrophilic to hydrophobic segments of the amphiphile played an imperative role in constructing lamellae. For example, hyperswollen lamellae was not naturally formed in aqueous solutions of $C_{12}E_6$. However, when a hydrophobic compound of styrene was added into the $C_{12}E_6$ solution, the hydrophobic part of self-assembly structures increased, thus resulting in the formation of lamellar phase. By the polymerization of styrene attached on the hydrophobic of $C_{12}E_6$, polystyrene nanosheets were formed in the interlayer of the hyperswollen lamellae. Besides, the appropriate mass ratio of the $C_{12}E_6$ to styrene monomer, suitable temperature, and fitted concentration of hydrophobic polymerization initiator were required to form the hyperswollen lamellar structures. As a typical example, $C_{12}E_6$-styrene system of hyperswollen lamellar phases was synthesized at the temperature ranging from 42 to 58 °C. The formed polystyrene nanosheets were thus converted into carbon nanosheets with aspect ratio of ~100 and average thickness of less than 2 nm by annealing treatment at 800 °C in N_2 gas [129].

Amphiphilic block copolymers

In comparison to small molecules, BCPs can form more robust assemblies due to their high molecular weight and entanglement of hydrophobic chains in the assemblies [130]. The robustness offers better stability to BCPs assemblies, which can maintain the aggregate morphology without serious transformation during the thermal treatment process. In addition, application of BCPs spherical micelles as pore-creating templates may generate mesopores in the resultant materials. In some typical energy devices such as LIBs and supercapacitors, carbon materials with mesoporous structures usually have better electrochemical performance in comparison with their microporous counterparts becasue the micropores that are too small may not be accessible to the electrolyte during charge and discharge processes. In contrast, smooth mass transport can be realized by using mesopores structure (pores size larger than 5 nm) [124]. As a typical example, a soft template approach was reported towards the fabrication of 2D ordered mesoporous carbon by close packing of BCPs micelles on various substrate, such as Si wafer and anodic aluminum oxide (AAO) membrane [131,132]. By using inner walls of the AAO channels as substrate (Fig. 10a), spherical monomicelles were prepared by solvent evaporation induced self-assembly of phenolic resol with pluronic triblock copolymer, and then deposited on the inner walls of AAO channels via electrostatic attractions. During the electrostatic attractions, these spherical monomicelles were continuously deposited and assembled into close-packing ordered micelles array, which were further transformed into bowl-like structures via in-situ polymerization and aggregation processes under hydrothermal conditions, eventually leading to the formation of polymer nanosheets with mesostructures. The mesoporous polymer nanosheets were further carbonized into the PCNs, which showed uniform mesopores structure with several micrometers in length, several hundred nanometers in width, and ~1 nm in thickness. Benefiting from the abundant ordered mesopores and large surface area, the 2D mesoporous nanosheets delivered initial discharge capacity of 3535 mAh g^{-1} at 100 mA g^{-1} and stabilized capacity of 770 mAh g^{-1} for LIBs. Even at a large current density of 5000 mA g^{-1}, the reversible capacity of 255 mAh g^{-1} was preserved [131]. The stabilized value of 770 mAh g^{-1} for 2D mesoporous nanosheets was higher than that of aforementioned porous FeS/C nanosheets (530 mA h g^{-1}), 2D

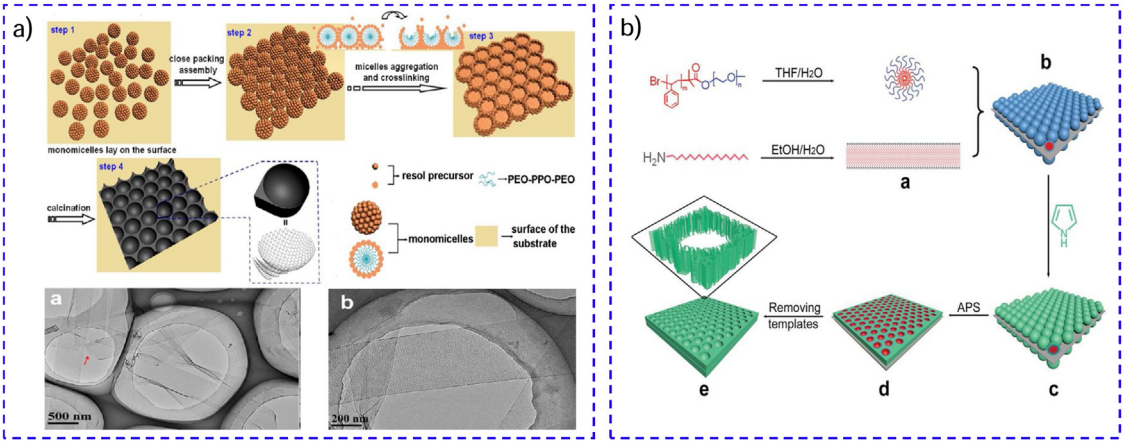

Fig. 10. Schematic illustration for (a) self-assembly of monomicelles towards 2D ordered mesoporous PCNs and corresponding typical TEM images (Reproduced with permission [131]. Copyright 2013, American Chemical Society), and (b) dual soft-templates synthesis of 2D mPPy nanosheets with controlled pore size, which can be converted to carbon nanosheets by pyrolysis. (Reproduced with permission [127]. Copyright 2016, Wiley-VCH).

ferrite/carbon hybrid (660 mAh g^{-1}), and graphitic PCNs (722 mAh g^{-1}), respectively. The same synthesis method was also applied to prepare 2D ordered mesoporous carbon/MoS_2 hybrid nanosheets by using MoS_2 monolayer as the substrate [133].

Recently, dual-templating strategy for the preparation of mesoporous mPPy nanosheets with tunable pore sizes was reported (Fig. 10b). In this strategy, synergic co-assembly of amphiphilic aliphatic amines (octadecylamine, OTA) and PS-b-PEO spherical micelles in solution generated a sandwich-like dual soft-templates structure, in which the micelles closely packed on both sides of the OTA lamella. Subsequently, pyrrole monomers were adsorbed in the PEO domains, and then polymerized into PPy polymer. Further removal of the templates by solvent extraction processing produced mPPy nanosheets with thickness of 25–30 nm, specific surface area of up to 96 $m^2 g^{-1}$, and tunable mesopore sizes ranging from 6.8 to 13.6 nm [127]. The dual-templating strategy was proved to be applicable for the fabrication of other types of conducting polymers. For example, ultrathin PANI (mPANI) nanosheets with periodic mesostructure were achieved, which showed a record high electricity conductivity of 41 S cm^{-1} among those of reported pristine PANI conducting polymers thus far [134]. These mPPy and mPANI nanosheets were considered to be readily converted to PCNs simply by thermal treatment.

Template-free method

Template-free method is an optional strategy to synthesize 2D carbon-based materials with no structual-directing agents in the synthesis approach. The precursors materials can spontaneously form 2D carbon frameworks in few facile steps, mainly including the pre-treatment of precusor and subsequent direct pyrolysis, which is different from hard template method and soft template method with relatively complicated protocols. Meanwhile, template-free method is able to employ broader range of available precursors than template methods. However, this template-free method exhibits the weakness in precise controlling the morphology and porous structure of achieved materials. In this part, several prominent examples of template-free synthesis of PCNs by employing different kinds of precursors involving small organic-molecules, polymer, and bio-mass are disscussed.

Small molecule precursors

The small organic molecules can be directly used as carbon precursors without any additional agents to prepare PCNs-based materials by formation of removable separation layers between the carbon nanosheets (Fig. 11). One-step thermal treatment is facile, economic, and eco-friendly strategy for the fabrication of PCNs via direct carbonization of a number of organic acid salts, including metal citrates and metal gluconates that are alternative molecular precursors. As a typical example, one-step carbonization procedure was employed to synthesize PCNs by using potassium citrate as precursor. The chemical reaction mechanism during this strategy was proposed as follows: the heating-treatment at temperature below 650 °C induced the decomposition of organic moiety in potassium citrate, resulting in the formation of porous carbon frameworks with inorganic impurities. After removal of the potassium inorganic compound by acid etching treatment, the PCNs consisting of rose-like particles were obtained, which had utrahigh specific surface area of up to 2220 $m^2 g^{-1}$ and thickness of 30–80 nm. By adjusting carbonization temperature, the surface area and micropore sizes of resultant PCNs materials could be further controlled. Especially, the specific surface area enlarged from 1360 to 2220 $m^2 g^{-1}$ when the annealing temperature was increased from 750 to 850 °C, and the pore size increased from 0.95 to 1.6 nm on elevating the annealing temperature was increased from 750 to 900 °C [135]. Similarly, some other small molecules such as magnesium citrate [136], sodium gluconate [137], oleic acid [138], sodium oleate [139], adamantane [140], and cheap organic solvents (ethylene glycol or glycerol [141,142]), have been also used as precursors to develop various 2D carbon-based materials. Briefly, with sodium gluconate as precursor, the PCNs with large aspect ratios of ~10^2-10^3 (length/thickness), thickness of 40–200 nm, and hierarchical microporous/mesoporous structures were prepared. When served as electrode material in supercapacitors, a specific capacitance as high as 140 F g^{-1} was attained for achieved PCNs nanosheets at 150,000 mA g^{-1} [137], slightly lower than that of the carbonized GHCPs (144 F g^{-1}).

Polymer precursors

2D sheet-like polymer and 3D polymer constructed by 2D nanostructures are alternative precursors for the fabrication of 2D carbon nanosheets and 3D carbon nanomaterials consisting of cabon nanosheets. There are various strategies to synthesize the polymer precusors involving solvothermal and direct polymerization methods. By changing the synthesis protocol of polymer precusors, the morphology, porous structure, and elemental compoistion of resulant carbon materials could be effectively adjusted. For example, a template-free synthesis strategy was developed for the construction of carbon superstructures consisting of fine-tunable nanosheets by using polyimide (PI) as precursors

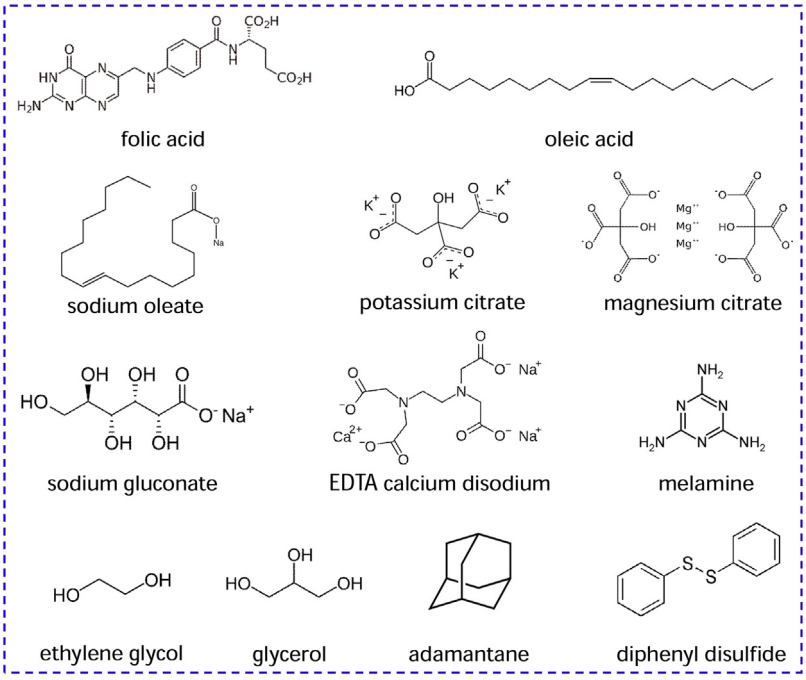

Fig. 11. Carbon-rich small organic molecules that have been used as precursors for preparation of PCNs materials.

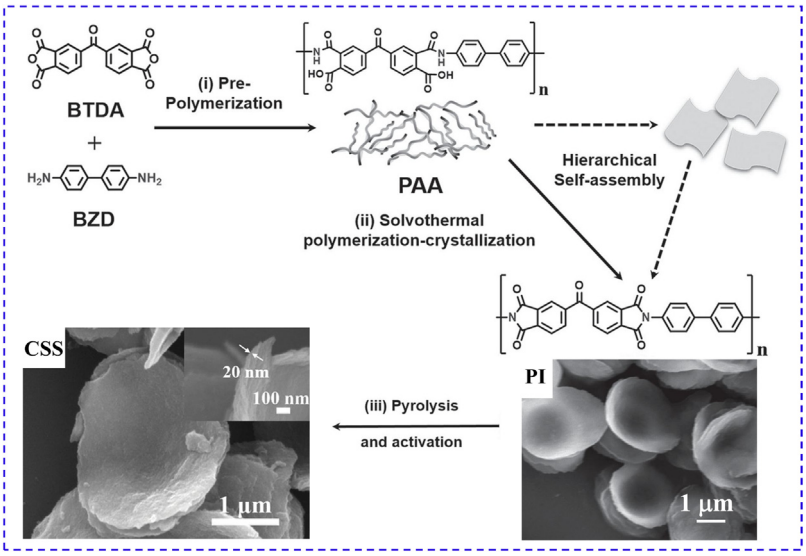

Fig. 12. Schematic illustration of the solvothermal method process approaching to polymer superstructures consisted of PI nanosheets and derived carbon superstructures. (Reproduced with permission [143]. Copyright 2016, Wiley-VCH).

(Fig. 12). The precursors were prepared by a solvothermal treatment of polyamic acid chains solution, and the results revealed that polymerization conditions, including the nature of solvent and concentration of polyamic acid chains, influenced the crystallization behavior of PI, thus resulting in the various unprecedented hierarchical superstructures, such as flower-like or lantern-shaped spheres. The mechanism for the formation of 3D polymer superstructures was proposed as below: the folding of linear PI chains by strong intermolecular forces firstly led to the formation of flat 2D nanosheets, which were then organized into 3D assemblies with different morphologies depending on the preparation conditions. After subsequent pyrolysis at 900 °C and NH_3 activation, PI-derived hierarchical structures involving lantern-shaped and flower-like spheres were converted to N-doped porous carbons (NPCs), which possessed N-doping content of up to 3.46%, specific surface area of 1375 $m^2 g^{-1}$, and hierarchical porous structures. Benefiting from the unique nanostructures, the as-prepared NPCs exhibited a remarkable catalytic activity with onset potential of up to 0.84 V and diffusion-limited current density of up to 5.5 mA cm^{-2} for ORR [143]. The high current density value of 5.5 mA cm^{-2} was superior to that of aforementioned M-CMPs-T material (5.4 mA cm^{-2}), B/N co-doped PCNs (4.5 mA cm^{-2}), and S/N-doped PCNs (4.0 mA cm^{-2}). Apart from the synthesized PI polymer superstructures, PI sheet-like structures and derived carbon nanosheets with ultrahigh surface area of 2607 $m^2 g^{-1}$ were also prepared via the similar polymer crystallization and subsquent carbonization treatment in molten salt [144].

Besides the solvothermal methods to prepare 2D sheet-like polymers, the strategies of self-polycondensation and/or condensation reaction were used to construct the 2D polymer frameworks

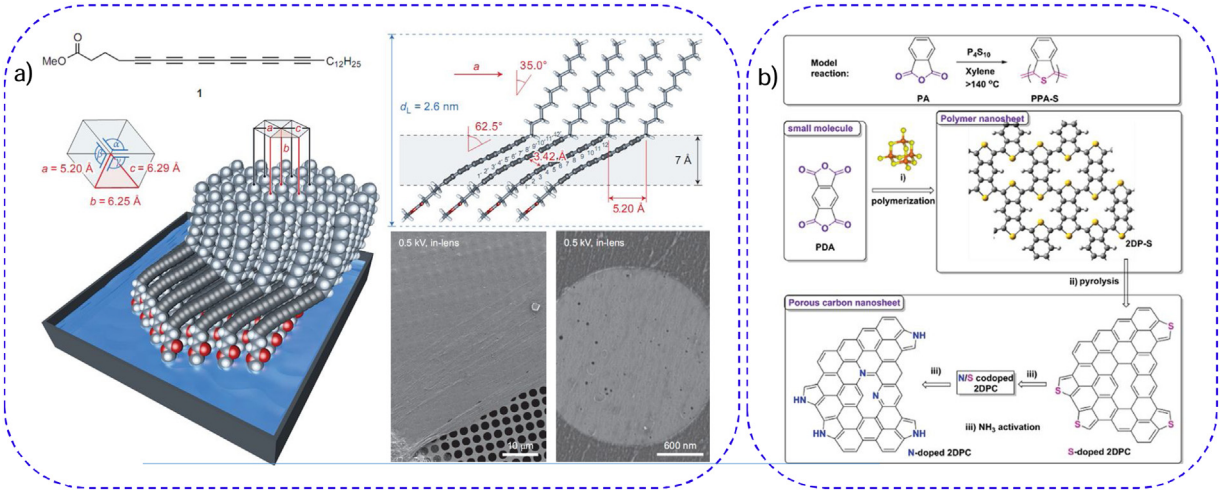

Fig. 13. Schematic illustration of the preparation routes for (a) functional carbon nanosheets synthesized by the self-assembly and subsequent carbonization of the hexayne amphiphile at air/water interface (Reproduced with permission [147]. Copyright 2014, Macmillan Publishers Limited), and (b) 2DP-S as precursor to prepare N/S dual-doped PCNs. (Reproduced with permission [148]. Copyright 2016, Wiley-VCH).

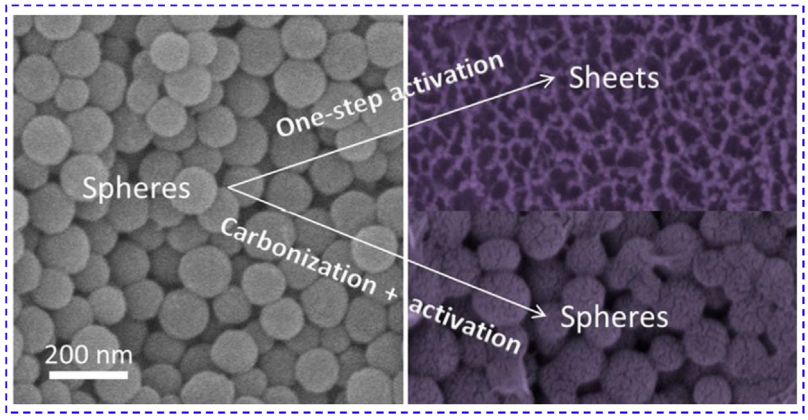

Fig. 14. Transformation of pGSs into the PCNs by one-step KOH activation. (Reproduced with permission [149]. Copyright 2014, American Chemical Society).

[145,146], which can be used as ideal precursors for the synthesis of PCNs. For example, a combined self-assembly of hexayne amphiphiles and ultraviolet-irradiated carbonization approach was developed for the "bottom-up" fabrication of functionalized carbon nanosheets (Fig. 13a). In this approach, the synthetic fatty acid ester amphiphiles served as monomers to form well-ordered self-assembled monolayers, which was the key step to further generate sp^2-rich carbon nanosheets with lateral dimension on the order of centimeters and thickness of 1.9 nm. This approach opens up promising possibilities for the preparation of carbon nanosheets derived from self-assembled polymer monolayers under mild conditions [147]. In addition, solution-based methods have been established to fabricate 2D sulfur-enriched conjugated polymers (2DP-S), in which 1,2,4,5-benzenetetracarboxylic anhydride was directly polymerized in anhydrous xylene in the presence of phosphorus pentasulfde (Fig. 13b). The resultant 2DP-S with ~7 nm in thickness and large aspect ratio of ~400 was further carbonized to N/S dual-doped PCNs (2D PCNs) by thermal treatment under NH_3 atmosphere. Acting as metal-free electrocatalysts for ORR, the as-prepared 2D PCNs delivered a 4-electron transfer mechanism and diffusion-limited current density of 5.1 mA cm^{-2} [148], which is slightly lower than that of NCNSs (5.2 mA cm^{-2}).

Apart from solvothermal and direct polymerization methods mentioned above, one-step synthetic process through carbonization and activation of polymer precursors even without layered structures has been reported to fabricate 2D carbon-based materials. For instance, PCNs were successfully synthesized by a facile chemical activation of polymerized glucose spheres (pGSs) by using KOH as activating agent. Compared with traditional precarbonization combined with activation treatment of pGSs that yielded microporous carbon spheres, the one-step activation method resulted in a dramatic morphological change from spheres to vertical oriented and interlinked sheet-like nanostructures (Fig. 14). The obtained PCNs provided ultrahigh specific surface area of 2633 $m^2 g^{-1}$, hierarchical porous structure (micropores of < 1 nm and mesopores of 5–10 nm), and high pore volume of 1.86 $cm^3 g^{-1}$. When served as the electrode material in supercapacitors [149], the resultant PCNs could reach a specific capacitance of 184 F g^{-1} at 100,000 mA g^{-1}, and the value of 184 F g^{-1} is over three times that of carbon spheres with microporous structure (56 F g^{-1}), with good long-term cyclic stability of 98% capacitance retainted after 2000 cycles at 1000 mA g^{-1}. Likewise, sulfur-doped PCNs (S-PCNs) was successfully prepared through a direct carbonization and KOH activation of Co-impregnated sulfonic acid ion exchange resin. The resultant S-PCNs had a thickness of ~4 nm, specific surface area of 2005 $m^2 g^{-1}$, and S-doping amount of 9.6 wt.% [150]. In addition to KOH that can serve as the activation agent, molten salts (e.g. LiCl/KCl and $NaBH_4$) were also reported as chemical agents to synthesize 2D PCNs based materials via the activation of polymer precursors [151–153].

Fig. 15. 2D PCNs-based materials derived from various bio-mass precursors.

Biomass precursors

Biomass materials, containing celluloses, hemicelluloses, lignins, biopolymers, proteins, etc., are abundant in nature and can be easily obtained. These biomass materials show various nanostructures including hierarchical porous structures, multilayer, few layer, and even monolayer structures [154]. Among them, biomass materials with multilevel layered structure have been applied for the preparation of diverse carbon-based nanosheets by thermal treatment and activation methods (Fig. 15) [155–157]. The resultant carbon materials are generally composed of interconnected porous nanosheets networks with high electrical conductivity and large surface area. In addition, this synthesis method has proven to be a green, economic, and desirable approach to form 2D carbon materials.

Plant biomass is one of popular precursors for the fabrication of PCNs. Typically, due to inheritance of the unique cellular structure inside this plant, peat moss have gained much interest. After a facile thermal treatment and activation process, the peat moss was converted into 3D carbon materials with interconnected macroporous network structure consisting of N-doped carbon nanosheets with ~60 nm in thickness [158]. As another example, hemp, which has been widely cultivated for centuries with traditional applications for paper, clothing, building material, and plastics industry, was also used for the preparation of PCNs. The PCNs with thickness

of 10–30 nm showed a high energy density of 40 Wh kg^{-1} when applied as electrode material for supercapacitors [159]. Furthermore, the N-doped PCNs can be synthesized via thermal annealing other types of natural plants, such as ginkgo leave [160], cornstalk [161], and brown seaweed [162].

Shell-type biomass materials, such as lobster shells [156], pistachio nutshells [163], coconut shells [164], and peanut skins [165], are also important precursors for the preparation of PCNs. For instance, using peanut skins as the carbon source, carbon nanosheets with tens of nanometer thickness (down to 20 nm), hierarchical micro-meso-macroporous architecture, and high specific surface area (2070 $m^2 g^{-1}$) were successfully prepared [165].

It is interesting that some popular foods in dailylife have been used as precursors for the synthesis of PCNs materials. By simple carbonization treatment of cassava, 3D carbon networks consisted of interconnected "honeycomb-like" cassava-carbon nanosheets interlayer were fabricated. When served as the polysulfides inhibitor in Li-S batteries, the resultant carbon materials exhibited specifc capacity as high as 811 mA h g^{-1} after 100 cycles at 0.5 C with 62% capacity retention [166]. However, after 100 cycles, only a discharge capacity of 324 mA h g^{-1} was preserved for 3D carbon networks without cassava-carbon sheets interlayers. The fruit-type materials involving sugarcanes [167] and citrus peels [168] were also applied in the fabrication of PCNs. By a simple carbonation and KOH activation treatment, the citrus peels were converted into N-doped porous carbon nanosheets with thickness of ~10 nm and numerous N/O heteroatoms (C/N and C/O ratios of 34.3 and 5.5).

Besides above-mentioned resources, some protein compounds and collagen-rich biomasses, such as pigskin [169], agar [170,171], gelatin [172–174], silk protein [175], and shellac biopolymer [176], have been also reported as precursors for the preparation of heteroatoms-doped PCNs. For instance, a carbonization and chemical activation treatment of collagen-rich pigskin precusor was utilized to produce N- and O- doped carbon nanosheets, which exhibited ultrahigh specific surface areas from 2209 to 3337 $m^2 g^{-1}$. By a simple carbonization of agar precusor that possessed high S content of 68.3 wt.%, vertically aligned and interconnected PCNs with thickness of 40–60 nm was successfully fabricated. When served as the electrode material in Li-S batteries, the 3D nanostructure presented a large initial discharge capacity of 1240 mAh g^{-1} at a current density of 167 mA g^{-1} and a reversible capacity of 844 mAh g^{-1} was maintained after 300 cycles [171]. The reversible specific capacity of the 3D nanostructure was much higher than those of aforementioned 3D carbon networks (62% and 811 mA h g^{-1}).

Conclusions and outlook

In summary, the recent progress on the synthetic strategies to produce PCNs and their hybrid materials were reviewed, and their promising electrochemical applications in energy storage and conversion devices were also highlighted. Different kinds of PCNs with controlled pore structures, aspect ratios, and specific surface areas have been prepared by various synthetic methods, including hard template strategy, soft template strategy, and template-free strategy. When these PCNs were employed as electrode/catalytic materials, they have shown great potential for the electrochemical applications in rechargeable lithium batteries, supercapacitors, and ORR electrocatalysis. Despites its outstanding physical and chemical properies, the ideal graphene itself is quite limited to be directly used as active material for energy applications, except after subsequent treatments, such as heteroatom doping and integrating with other active materials. Inspired by this concern, the PCNs not only can be designed and prepared with controlled heteroatom/metal dopants and embedded active particles, but also be adjusted by post treatment under various conditions, such as hydrothermal process, plasma treatment, NH_3 activation, electrochemical depositing, chemical vapor deposition, atomic layer deposition, etc. Although many kinds of methods, precursors, and templates have already been developed for the synthesis of PCNs with promising electrochemical performance in energy energy storage and conversion applications, several kinds of targeted PCNs materials still remain important challenges, such as (1) PCNs with controlled and ordered micropore/mesopore structures, (2) PCNs with ultra-high specific surface areas (> 3000 $m^2 g^{-1}$), (3) PCNs with ultra-high pore volume, (4) PCNs with uniform morphology or dimensionality control, etc.

At the current stage, most these reported works mainly focused on the development of the synthetic methods towards the preparation of PCNs. Using of these 2D carbon nanosheets as starting materials to construct new functional materials or new structures, such as (1) 3D hierarchical porous carbon materials, (2) free-standing 2D heterostructures, and (3) thickness-controlled polymer films, is still rarely reported. The poor solvent dispersibility of PCNs is now hindering the rapid development of PCNs-based materials, which may be solved by covalent or non-covalent functionalization in the future. A great effort will be devoted to develop new methods towards the preparation of PCNs and new kinds of PCNs based materials, meanwhile expanding the application range of such PCNs materials in separation membranes, biochemical sensors, and quantum devices, etc.

Acknowledgements

Y. Hou gratefully acknowledges the financial support of National Natural Science Foundation of China (51702284 and 21878270), the Startup Foundation for Hundred-Talent Program of Zhejiang University (112100-193820101/001/022), and Zhejiang Provincial Natural Science Foundation of China (LR19B060002). Y. Mai acknowledges National Natural Science Foundation of China (51573091, 21774076, 21320102006, and 91527304) and Program of the Shanghai Committee of Science and Technology (17JC1403200). X. Feng acknowledges the EC under the Graphene Flagship (CNECT-ICT-604391), UP-GREEN, the ERC Grant 2DMATER, the CFAED, and National Natural Science Foundation of China (21720102002). X. Zhuang acknowledges National Natural Science Foundation of China (51722304).

References

[1] Y. Shi, L. Peng, Y. Ding, Y. Zhao, G. Yu, Chem. Soc. Rev. 44 (2015) 6684–6696.
[2] Z.L. Wang, D. Xu, J.J. Xu, X.B. Zhang, Chem. Soc. Rev. 43 (2014) 7746–7786.
[3] Y. Hou, J. Li, Z. Wen, S. Cui, C. Yuan, J. Chen, Nano Energy 12 (2015) 1–8.
[4] T. Lv, M. Liu, D. Zhu, L. Gan, T. Chen,Adv. Mater. 30 (2018), 1705489.
[5] Q. Meng, K. Cai, Y. Chen, L. Chen, Nano Energy 36 (2017) 268–285.
[6] S.F. Fu, C.Z. Zhu, J.H. Song, D. Du, Y.H. Lin,Adv. Energy Mater. 7 (2017), 1700363.
[7] A. Kulkarni, S. Siahrostami, A. Patel, J.K. Nørskov, Chem. Rev. 118 (2018) 2302–2312.
[8] Y. Hou, T. Huang, Z. Wen, S. Mao, S. Cui, J. Chen,Adv. Energy Mater. 4 (2014), 1400337.
[9] S.Y. Lim, W. Shen, Z. Gao, Chem. Soc. Rev. 44 (2015) 362–381.
[10] S. Pedireddy, H.K. Lee, W.W. Tjiu, I.Y. Phang, H.R. Tan, S.Q. Chua, C. Troadec, X.Y. Ling, Nat. Commun. 5 (2014) 4947.
[11] G. Ciric-Marjanovic, I. Pasti, S. Mentus, Prog. Mater. Sci. 69 (2015) 61–182.
[12] C. Sun, Q. Xu, Y. Xie, Y. Ling, Y. Hou, J. Mater. Chem. A Mater. Energy Sustain. 6 (2018) 8289–8298.
[13] Z. Li, G. Li, X. Chen, Z. Xia, J. Yao, B. Yang, L. Lei, Y. Hou, ChemSusChem 11 (2018) 2382–2387.
[14] Y. Hou, X.Y. Li, Q.D. Zhao, X. Quan, G.H. Chen, Adv. Funct. Mater. 20 (2010) 2165–2174.
[15] Y. Hou, X. Li, Q. Zhao, X. Quan, G. Chen, J. Mater. Chem. 21 (2011) 18067–18076.
[16] Y. Hou, F. Zuo, A. Dagg, P. Feng, Angew. Chem. Int. Ed. 125 (2013) 1286–1290.
[17] X. Zheng, J. Luo, W. Lv, D.W. Wang, Q.H. Yang, Adv. Mater. 27 (2015) 5388–5395.
[18] Y. Hou, X. Zhuang, X. Feng,Small Methods 1 (2017), 1700090.
[19] Y. Hou, S. Cui, Z. Wen, X. Guo, X. Feng, J. Chen, Small 11 (2015) 5940–5948.

[20] A.D. Roberts, X. Li, H. Zhang, Chem. Soc. Rev. 43 (2014) 4341–4356.
[21] Y. Hou, M. Qiu, T. Zhang, J. Ma, S. Liu, X. Zhuang, C. Yuan, X. Feng,Adv. Mater. 29 (2017), 1604480.
[22] Y. Hou, Z. Wen, S. Cui, X. Feng, J. Chen, Nano Lett. 16 (2016) 2268–2277.
[23] H. Tian, Z. Lin, F. Xu, J. Zheng, X. Zhuang, Y. Mai, X. Feng, Small 12 (2016) 3155–3163.
[24] J.F. Ni, Y. Li,Adv. Energy Mater. 6 (2016), 1600278.
[25] X. Zhuang, D. Gehrig, N. Forler, H. Liang, M. Wagner, M.R. Hansen, F. Laquai, F. Zhang, X. Feng, Adv. Mater. 27 (2015) 3789–3796.
[26] Y. Hou, M. Qiu, G. Nam, M.G. Kim, T. Zhang, K. Liu, X. Zhuang, J. Cho, C. Yuan, X. Feng, Nano Lett. 17 (2017) 4202–4209.
[27] Y. Hou, M. Qiu, T. Zhang, X. Zhuang, C.S. Kim, C. Yuan, X. Feng,Adv. Mater. 29 (2017), 1701589.
[28] Y. Hou, M.R. Lohe, J. Zhang, S. Liu, X. Zhuang, X. Feng, Energy Environ. Sci. 9 (2016) 478–483.
[29] F. Bonaccorso, L. Colombo, G. Yu, M. Stoller, V. Tozzini, A.C. Ferrari, R.S. Ruoff, V. Pellegrini,Science 347 (2015), 1246501.
[30] M. Batmunkh, M. Bat-Erdene, J.G. Shapter,Adv. Energy Mater. 8 (2018), 1701832.
[31] R. Lv, J.A. Robinson, R.E. Schaak, D. Sun, Y. Sun, T.E. Mallouk, M. Terrones, Acc. Chem. Res. 48 (2015) 56–64.
[32] G. Fan, F. Li, D.G. Evans, X. Duan, Chem. Soc. Rev. 43 (2014) 7040–7066.
[33] J. Tucek, P. Blonski, J. Ugolotti, A.K. Swain, T. Enoki, R. Zboril, Chem. Soc. Rev. 47 (2018) 3899–3990.
[34] A. Vasileff, Y. Zheng, S.Z. Qiao,Adv. Energy Mater. 7 (2017), 1700759.
[35] X. Wang, A. Vasileff, Y. Jiao, Y. Zheng, S.Z. Qiao,Adv. Mater. (2018), 1803625.
[36] M.M. Titirici, R.J. White, N. Brun, V.L. Budarin, D.S. Su, F. del Monte, J.H. Clark, M.J. MacLachlan, Chem. Soc. Rev. 44 (2015) 250–290.
[37] L. Hao, X. Li, L. Zhi, Adv. Mater. 25 (2013) 3899–3904.
[38] Z. Niu, L. Liu, L. Zhang, X. Chen, Small 10 (2014) 3434–3441.
[39] W.J. Yuan, J. Chen, G.Q. Shi, Mater. Today 17 (2014) 77–85.
[40] Y. Sakamoto, M. Kaneda, O. Terasaki, D.Y. Zhao, J.M. Kim, G. Stucky, H.J. Shin, R. Ryoo, Nature 408 (2000) 449–453.
[41] G. Wu, A. Santandreua, W. Kellogga, S. Gupta, O. Ogokea, H. Zhang, H.L. Wang, L. Dai, Nano Energy 29 (2016) 83–110, 29.
[42] P. Simon, Y. Gogotsi, Nat. Mater. 7 (2008) 845–854.
[43] F. Schüth, W. Schmidt, Adv. Mater. 14 (2002) 629–638.
[44] H. Zhang, J. Li, Q. Tan, L. Lu, Z. Wang, G. Wu, Chem. Eur. J. 24 (2018) 1–22.
[45] J. Lee, J. Kim, T. Hyeon, Adv. Mater. 18 (2006) 2073–2094.
[46] C. Liang, Z. Li, S. Dai, Angew. Chem. Int. Ed. 47 (2008) 3696–3717.
[47] H. Jiang, P.S. Lee, C.Z. Li, Energy Environ. Sci. 6 (2013) 41–53.
[48] X.W. Lou, L.A. Archer, Z.C. Yang, Adv. Mater. 20 (2008) 3987–4019.
[49] Z. Li, H.B. Wu, X.W. Lou, Energy Environ. Sci. 9 (2016) 3061–3070.
[50] P. Kissel, R. Erni, W.B. Schweizer, M.D. Rossell, B.T. King, T. Bauer, S. Gotzinger, A.D. Schluter, J. Sakamoto, Nat. Chem. 4 (2012) 287–291.
[51] Y.W. Peng, W.K. Wong, Z.G. Hu, Y.D. Cheng, D.Q. Yuan, S.A. Khan, D. Zhao, Chem. Mater. 28 (2016) 5095–5101.
[52] F. Xie, L. Zhang, D. Su, M. Jaroniec, S.Z. Qiao,Adv. Mater. 29 (2017), 1700989.
[53] H.L. Qian, C.X. Yang, X.P. Yan, Nat. Commun. 7 (2016) 12104.
[54] J. Lu, R. Cao, Angew. Chem. Int. Ed. 55 (2016) 9474–9480.
[55] J. Wang, Y. Xu, B. Ding, Z. Chang, X. Zhang, Y. Yamauchi, K.C.W. Wu, Angew. Chem. Int. Ed. 57 (2018) 2894–2898.
[56] K. Peng, H. Yang, Chem. Commun. 53 (2017) 6085–6088.
[57] H.W. Liang, W. Wei, Z.S. Wu, X. Feng, K. Mullen, J. Am. Chem. Soc. 135 (2013) 16002–16005.
[58] J. Gong, J. Liu, X.C. Chen, Z.W. Jiang, X. Wen, E. Mijowska, T. Tang, J. Mater. Chem. A Mater. Energy Sustain. 3 (2015) 341–351.
[59] J. Gong, B. Michalkiewicz, X.C. Chen, E. Mijowska, J. Liu, Z.W. Jiang, X. Wen, T. Tang, ACS Sustain. Chem. Eng. 2 (2014) 2837–2844.
[60] X.D. Guo, G.L. Liu, S. Yue, J. He, L.Y. Wang, RSC Adv. 5 (2015) 96062–96066.
[61] R. Atchudan, S. Perumal, T.N.J.I. Edison, Y.R. Lee, RSC Adv. 5 (2015) 93364–93373.
[62] A.P. Wang, F.Y. Kang, Z.H. Huang, Z.C. Guo, X.Y. Chuan, Microporous Mesoporous Mater. 108 (2008) 318–324.
[63] M. Opanasenko, W.O. Parker Jr., M. Shamzhy, E. Montanari, M. Bellettato, M. Mazur, R. Millini, J. Cejka, J. Am. Chem. Soc. 136 (2014) 2511–2519.
[64] X. Xiao, H. Yu, H. Jin, M. Wu, Y. Fang, J. Sun, Z. Hu, T. Li, J. Wu, L. Huang, Y. Gogotsi, J. Zhou, ACS Nano 11 (2017) 2180–2186.
[65] X. Xiao, H. Song, S. Lin, Y. Zhou, X. Zhan, Z. Hu, Q. Zhang, J. Sun, B. Yang, T. Li, L. Jiao, J. Zhou, J. Tang, Y. Gogotsi, Nat. Commun. 7 (2016) 11296.
[66] H. Lei, T.T. Yan, H. Wang, L.Y. Shi, J.P. Zhang, D.S. Zhang, J. Mater. Chem. A Mater. Energy Sustain. 3 (2015) 5934–5941.
[67] H. Peng, G.F. Ma, K.J. Sun, J.J. Mu, Z.Q. Lei, J. Mater. Chem. A Mater. Energy Sustain. 2 (2014) 17297–17301.
[68] Y.Q. Yang, J.A. Zhang, X.C. Wu, Y.S. Fu, H.X. Wu, S.W. Guo, J. Mater. Chem. A Mater. Energy Sustain. 2 (2014) 9111–9117.
[69] R.R. Song, H.H. Song, X.H. Chen, Y. Cui, J.S. Zhou, S. Zhang, Electrochim. Acta 127 (2014) 186–192.
[70] R.R. Song, H.H. Song, J.S. Zhou, X.H. Chen, B. Wu, H.Y. Yang, J. Mater. Chem. 22 (2012) 12369–12374.
[71] D. Liu, X. Wang, X. Wang, W. Tian, J. Liu, C. Zhi, D. He, Y. Bando, D. Golberg, J. Mater. Chem. A 1 (2013) 1952.
[72] B. Jang, M. Park, O.B. Chae, S. Park, Y. Kim, S.M. Oh, Y. Piao, T. Hyeon, J. Am. Chem. Soc. 134 (2012) 15010–15015.
[73] G.T. Fu, Z.M. Cui, Y.F. Chen, Y.T. Li, Y.W. Tang, J.B. Goodenough,Adv. Energy Mater. 7 (2017), 1601172.
[74] L. Chen, Z. Wang, C. He, N. Zhao, C. Shi, E. Liu, J. Li, ACS Appl. Mater. Interfaces 5 (2013) 9537–9545.
[75] Y.X. Xu, W.Y. Li, F. Zhang, X.L. Zhang, W.J. Zhang, C.S. Lee, Y.B. Tang, J. Mater. Chem. A 4 (2016) 3697–3703.
[76] J. Ma, Y.Z. Dong, L. Wang, P. Yu, H.J. Yan, C.G. Tian, J.H. Li, H.G. Fu, ChemistrySelect 1 (2016) 2167–2173.
[77] S. Zhu, J. Li, L. Ma, L. Guo, Q. Li, C. He, E. Liu, F. He, C. Shi, N. Zhao, ACS Appl. Mater. Interfaces 8 (2016) 11720–11728.
[78] J. Zhu, K. Sakaushi, G. Clavel, M. Shalom, M. Antonietti, T.P. Fellinger, J. Am. Chem. Soc. 137 (2015) 5480–5485.
[79] R. Raccichini, A. Varzi, S. Passerini, B. Scrosati, Nat. Mater. 14 (2015) 271–279.
[80] Y. Hou, Z.H. Wen, S.M. Cui, S.Q. Ci, S. Mao, J.H. Chen, Adv. Funct. Mater. 25 (2015) 872–882.
[81] Y. Hou, F. Zuo, A. Dagg, P. Feng, Nano Lett. 12 (2012) 6464–6473.
[82] Y. Hou, F. Zuo, Q. Ma, C. Wang, L. Bartels, P.Y. Feng, J. Phys. Chem. C 116 (2012) 20132–20139.
[83] Z. Li, S. Wu, W. Lv, J.J. Shao, F. Kang, Q.H. Yang, Small 12 (2016) 2674–2688.
[84] S. Zhu, H. Tian, N. Wang, B. Chen, Y. Mai, X. Feng,Small 14 (2018), 1702755.
[85] C. Chung, Y.K. Kim, D. Shin, S.R. Ryoo, B.H. Hong, D.H. Min, Acc. Chem. Res. 46 (2013) 2211–2224.
[86] A. Cannavale, P. Cossari, G.E. Eperon, S. Colella, F. Fiorito, G. Gigli, H.J. Snaith, A. Listorti, Energy Environ. Sci. 9 (2016) 2682–2719.
[87] C. Lu, D. Tranca, J. Zhang, F.N. Rodri Guez Hernandez, Y. Su, X. Zhuang, F. Zhang, G. Seifert, X. Feng, ACS Nano 11 (2017) 3933–3942.
[88] C.B. Lu, S.H. Liu, F. Zhang, Y.Z. Su, X.X. Zou, Z. Shi, G.D. Li, X.D. Zhuang, J. Mater. Chem. A 5 (2017) 1567–1574.
[89] X. Chen, Z.B. Xiao, X.T. Ning, Z. Liu, Z. Yang, C. Zou, S. Wang, X.H. Chen, Y. Chen, S.M. Huang,Adv. Energy Mater. 4 (2014), 1301988.
[90] S. Yang, X. Feng, X. Wang, K. Mullen, Angew. Chem. Int. Ed. 50 (2011) 5339–5343.
[91] W. Wei, H. Liang, K. Parvez, X. Zhuang, X. Feng, K. Mullen, Angew. Chem. Int. Ed. 53 (2014) 1570–1574.
[92] W. Wei, G. Wang, S. Yang, X. Feng, K. Mullen, J. Am. Chem. Soc. 137 (2015) 5576–5581.
[93] B.P. Bastakoti, M. Inuoe, S.I. Yusa, S.H. Liao, K.C.W. Wu, K. Nakashima, Y. Yamauchi, Chem. Commun. 48 (2012) 6532–6534.
[94] M.Q. Li, C.K. Ober, Mater. Today 9 (2006) 30–39.
[95] S. Liu, P. Gordiichuk, Z.S. Wu, Z. Liu, W. Wei, M. Wagner, N. Mohamed-Noriega, D. Wu, Y. Mai, A. Herrmann, K. Mullen, X. Feng, Nat. Commun. 6 (2015) 8817.
[96] L. Borchardt, Q.L. Zhu, M.E. Casco, R. Berger, X. Zhuang, S. Kaskel, X. Feng, Q. Xu, Mater. Today 20 (2017) 592–610.
[97] F. Xu, D. Wu, R. Fu, B. Wei, Mater.Today 20 (2017) 629–656.
[98] K. Yuan, T. Hu, Y.Z. Xu, R. Graf, G. Brunklaus, M. Forster, Y.W. Chen, U. Scherf, ChemElectroChem 3 (2016) 822–828.
[99] J.H. Zhu, X.D. Zhuang, J. Yang, X.L. Feng, S. Hirano, J. Mater. Chem. A 5 (2017) 16732–16739.
[100] C.A. Cao, X.D. Zhuang, Y.Z. Su, Y. Zhang, F. Zhang, D.Q. Wu, X.L. Feng, Polym. Chem. 5 (2014) 2057–2064.
[101] W.X. Zhao, Z.S. Hou, Z.Q. Yao, X.D. Zhuang, F. Zhang, X.L. Feng, Polym. Chem. 6 (2015) 7171–7178.
[102] L. Wang, Y. Wan, Y. Ding, S. Wu, Y. Zhang, X. Zhang, G. Zhang, Y. Xiong, X. Wu, J. Yang, H. Xu,Adv. Mater. 29 (2017), 1702428.
[103] Y. Xu, S. Jin, H. Xu, A. Nagai, D. Jiang, Chem. Soc. Rev. 42 (2013) 8012–8031.
[104] X. Zhuang, F. Zhang, D. Wu, N. Forler, H. Liang, M. Wagner, D. Gehrig, M.R. Hansen, F. Laquai, X. Feng, Angew. Chem. Int. Ed. 52 (2013) 9668–9672.
[105] Y. Zhang, X. Zhuang, Y. Su, F. Zhang, X. Feng, J. Mater. Chem. A 2 (2014) 7742–7746.
[106] X. Zhuang, F. Zhang, D. Wu, X. Feng, Adv. Mater. 26 (2014) 3081–3086.
[107] Q. Wang, J. Yan, T. Wei, J. Feng, Y.M. Ren, Z.J. Fan, M.L. Zhang, X.Y. Jing, Carbon 60 (2013) 481–487.
[108] Z.J. Fan, Y. Liu, J. Yan, G.Q. Ning, Q. Wang, T. Wei, L.J. Zhi, F. Wei, Adv. Energy Mater. 2 (2012) 419–424.
[109] Z.M. Zheng, X. Zhang, F. Pei, Y. Dai, X.L. Fang, T.H. Wang, N.F. Zheng, J. Mater. Chem. A 3 (2015) 19800–19806.
[110] L. Peng, Y.Y. Feng, Y.J. Bai, H.J. Qiu, Y. Wang, J. Mater. Chem. A 3 (2015) 8825–8831.
[111] H.J. Wang, L.Q. Zhi, K.Q. Liu, L.Q. Dang, Z.H. Liu, Z.B. Lei, C. Yu, J.S. Qiu, Adv. Funct. Mater. 25 (2015) 5420–5427.
[112] J. Duan, S. Chen, M. Jaroniec, S.Z. Qiao, ACS Nano 9 (2015) 931–940.
[113] Y.N. Zhu, C.Y. Cao, W.J. Jiang, S.L. Yang, J.S. Hu, W.G. Song, L.J. Wan, J. Mater. Chem. A 4 (2016) 18470–18477.
[114] H. Yu, L. Shang, T. Bian, R. Shi, G.I. Waterhouse, Y. Zhao, C. Zhou, L.Z. Wu, C.H. Tung, T. Zhang, Adv. Mater. 28 (2016) 5080–5086.
[115] Y. Hou, Z. Wen, S. Cui, X. Guo, J. Chen, Adv. Mater. 25 (2013) 6291–6297.
[116] M. Chhowalla, Z. Liu, H. Zhang, Chem. Soc. Rev. 44 (2015) 2584–2586.
[117] M. Chhowalla, H.S. Shin, G. Eda, L.J. Li, K.P. Loh, H. Zhang, Nat. Chem. 5 (2013) 263–275.
[118] X. Cao, C. Tan, X. Zhang, W. Zhao, H. Zhang, Adv. Mater. 28 (2016) 6167–6196.
[119] X. Chia, A.Y.S. Eng, A. Ambrosi, S.M. Tan, M. Pumera, Chem. Rev. 115 (2015) 11941–11966.
[120] Y. Hou, B. Zhang, Z. Wen, S. Cui, X. Guo, Z. He, J. Chen, J. Mater. Chem. A 2 (2014) 13795–13800.
[121] Y. Hou, J. Li, Z. Wen, S. Cui, C. Yuan, J. Chen, Nano Energy 8 (2014) 157–164.

[122] H. Tian, S. Zhu, F. Xu, W. Mao, H. Wei, Y. Mai, X. Feng, ACS Appl. Mater. Interfaces 9 (2017) 43975–43982.
[123] K. Yuan, X. Zhuang, H. Fu, G. Brunklaus, M. Forster, Y. Chen, X. Feng, U. Scherf, Angew. Chem. Int. Ed. 55 (2016) 6858–6863.
[124] Y. Deng, J. Wei, Z. Sun, D. Zhao, Chem. Soc. Rev. 42 (2013) 4054–4070.
[125] Z. Lin, S. Liu, W. Mao, H. Tian, N. Wang, N. Zhang, F. Tian, L. Han, X. Feng, Y. Mai, Angew. Chem. Int. Ed. 56 (2017) 7135–7140.
[126] Y.P. Zhu, S.Z. Qiao, Nanoscale 9 (2017) 18731–18736.
[127] S. Liu, F. Wang, R. Dong, T. Zhang, J. Zhang, X. Zhuang, Y. Mai, X. Feng, Adv. Mater. 28 (2016) 8365–8370.
[128] H. Tian, N. Wang, F.G. Xu, P.F. Zhang, D. Hou, Y.Y. Mai, X.L. Feng, J. Mater. Chem. A 6 (2018) 10354–10360.
[129] Y. Uchida, T. Nishizawa, T. Omiya, Y. Hirota, N. Nishiyama, J. Am. Chem. Soc. 138 (2016) 1103–1105.
[130] K. Vijayan, D.E. Discher, J. Polym. Sci. Pol. Phys. 44 (2006) 3431–3433.
[131] Y. Fang, Y. Lv, R. Che, H. Wu, X. Zhang, D. Gu, G. Zheng, D. Zhao, J. Am. Chem. Soc. 135 (2013) 1524–1530.
[132] Y. Fang, Y. Lv, J. Tang, H. Wu, D. Jia, D. Feng, B. Kong, Y. Wang, A.A. Elzatahry, D. Al-Dahyan, Q. Zhang, G. Zheng, D. Zhao, Angew. Chem. Int. Ed. 54 (2015) 8425–8429.
[133] Y. Fang, Y. Lv, F. Gong, A.A. Elzatahry, G. Zheng, D. Zhao, Adv. Mater. 28 (2016) 9385–9390.
[134] S. Liu, J. Zhang, R. Dong, P. Gordiichuk, T. Zhang, X. Zhuang, Y. Mai, F. Liu, A. Herrmann, X. Feng, Angew. Chem. Int. Ed. 55 (2016) 12516–12521.
[135] M. Sevilla, A.B. Fuertes, ACS Nano 8 (2014) 5069–5078.
[136] X. Yu, J. Zhao, R. Lv, Q. Liang, C. Zhan, Y. Bai, Z.H. Huang, W. Shen, F. Kang, J. Mater. Chem. A 3 (2015) 18400–18405.
[137] A.B. Fuertes, M. Sevilla, ACS Appl. Mater. Interfaces 7 (2015) 4344–4353.
[138] L. Zhang, H.P. Guo, R. Rajagopalan, X.L. Hu, Y.H. Huang, S.X. Dou, H.K. Liu, J. Mater. Chem. A 4 (2016) 4056–4061.
[139] W. Fu, F.H. Du, K.X. Wang, T.N. Ye, X. Wei, J.S. Chen, J. Mater. Chem. A 2 (2014) 6960–6965.
[140] A.Y. Jee, M. Lee, Carbon 47 (2009) 2546–2548.
[141] Y. Chang, M. Antonietti, T.P. Fellinger, Angew. Chem. Int. Ed. 54 (2015) 5507–5512.
[142] W.T. Wang, S. Chakrabarti, Z.G. Chen, Z.F. Yan, M.O. Tade, J. Zou, Q. Li, J. Mater. Chem. A 2 (2014) 2390–2396.
[143] Z. Xu, X. Zhuang, C. Yang, J. Cao, Z. Yao, Y. Tang, J. Jiang, D. Wu, X. Feng, Adv. Mater. 28 (2016) 1981–1987.
[144] P.F. Zhang, Z.A. Qiao, Z.Y. Zhang, S. Wan, S. Dai, J. Mater. Chem. A 2 (2014) 12262–12269.
[145] Z. Xiang, Y. Xue, D. Cao, L. Huang, J.F. Chen, L. Dai, Angew. Chem. Int. Ed. 53 (2014) 2433–2437.
[146] X. Zhuang, W. Zhao, F. Zhang, Y. Cao, F. Liu, S. Bi, X. Feng, Polym. Chem. 7 (2016) 4176–4181.
[147] S. Schrettl, C. Stefaniu, C. Schwieger, G. Pasche, E. Oveisi, Y. Fontana, A. Fontcuberta i Morral, J. Reguera, R. Petraglia, C. Corminboeuf, G. Brezesinski, H. Frauenrath, Nat. Chem. 6 (2014) 468–476.
[148] Y.Z. Su, Z.Q. Yao, F. Zhang, H. Wang, Z. Mics, E. Canovas, M. Bonn, X.D. Zhuang, X.L. Feng, Adv. Funct. Mater. 26 (2016) 5893–5902.
[149] X. Zheng, W. Lv, Y. Tao, J. Shao, C. Zhang, D. Liu, J. Luo, D.W. Wang, Q.H. Yang, Chem. Mater. 26 (2014) 6896–6903.
[150] W.F. Deng, Y.J. Zhang, L. Yang, Y.M. Tan, M. Ma, Q.J. Xie, RSC Adv. 5 (2015) 13046–13051.
[151] X.F. Liu, M. Antonietti, Carbon 69 (2014) 460–466.
[152] B. He, W.C. Li, A.H. Lu, J. Mater. Chem. A 3 (2015) 579–585.
[153] X. Lin, X. Li, F. Li, Y. Fang, M. Tian, X. An, Y. Fu, J. Jin, J. Ma, J. Mater. Chem. A 4 (2016) 6505–6512.
[154] W. Long, B. Fang, A. Ignaszak, Z. Wu, Y.J. Wang, D. Wilkinson, Chem. Soc. Rev. 46 (2017) 7176–7190.
[155] J. Hou, C. Cao, F. Idrees, X. Ma, ACS Nano 9 (2015) 2556–2564.
[156] Q. Liu, Y. Duan, Q. Zhao, F. Pan, B. Zhang, J. Zhang, Langmuir 30 (2014) 8238–8245.
[157] T. Wu, G. Wang, Q. Dong, F. Zhan, X. Zhang, S. Li, H. Qiao, J. Qiu, Environ. Sci. Technol. 51 (2017) 9244–9251.
[158] J. Ding, H. Wang, Z. Li, A. Kohandehghan, K. Cui, Z. Xu, B. Zahiri, X. Tan, E.M. Lotfabad, B.C. Olsen, D. Mitlin, ACS Nano 7 (2013) 11004–11015.
[159] H. Wang, Z. Xu, A. Kohandehghan, Z. Li, K. Cui, X. Tan, T.J. Stephenson, C.K. King'ondu, C.M. Holt, B.C. Olsen, J.K. Tak, D. Harfield, A.O. Anyia, D. Mitlin, ACS Nano 7 (2013) 5131–5141.
[160] F.P. Pan, Z.Y. Cao, Q.P. Zhao, H.Y. Liang, J.Y. Zhang, J. Power Sources 272 (2014) 8–15.
[161] L. Wang, G. Mu, C. Tian, L. Sun, W. Zhou, P. Yu, J. Yin, H. Fu, ChemSusChem 6 (2013) 880–889.
[162] W. Cui, N. Cheng, Q. Liu, C. Ge, A.M. Asiri, X. Sun, ACS Catal. 4 (2014) 2658–2661.
[163] J. Xu, Q. Gao, Y. Zhang, Y. Tan, W. Tian, L. Zhu, L. Jiang, Sci. Rep. 4 (2014) 5545.
[164] L. Wang, L. Zhao, P. Yu, C.G. Tian, F.F. Sun, H. Feng, W. Zhou, J.Q. Wang, H.G. Fu, J. Mater. Chem. A 3 (2015) 24139–24147.
[165] H. Wang, D. Mitlin, J. Ding, Z. Li, K. Cui, J. Mater. Chem. A 4 (2016) 5149–5158.
[166] F.R. Qin, K. Zhang, J. Fang, Y.Q. Lai, Q. Li, Z.A. Zhang, J. Li, New J. Chem. 38 (2014) 4549–4554.
[167] M. Yang, Y.R. Zhong, X.L. Zhou, J.J. Ren, L.W. Su, J.P. Wei, Z. Zhou, J. Mater. Chem. A 2 (2014) 12519–12525.
[168] N.R. Kim, Y.S. Yun, M.Y. Song, S.J. Hong, M. Kang, C. Leal, Y.W. Park, H.J. Jin, ACS Appl. Mater. Interfaces 8 (2016) 3175–3181.
[169] Y. Wang, R. Yang, Y. Wei, Z.J. Zhao, M. Li, RSC Adv. 4 (2014) 45318–45324.
[170] S.W. Zhang, M.Y. Zeng, J.X. Li, J. Li, J.Z. Xu, X.K. Wang, J. Mater. Chem. A 2 (2014) 4391–4397.
[171] S. Rehman, X.X. Gu, K. Khan, N. Mahmood, W.L. Yang, X.X. Huang, S.J. Guo, Y.L. Hou,Adv. Energy Mater. 6 (2016), 1502518.
[172] X.M. Fan, C. Yu, J. Yang, Z. Ling, C. Hu, M.D. Zhang, J.S. Qiu,Adv. Energy Mater. 5 (2015), 1401761.
[173] Z. Ling, Z.Y. Wang, M.D. Zhang, C. Yu, G. Wang, Y.F. Dong, S.H. Liu, Y.W. Wang, J.S. Qiu, Adv. Funct. Mater. 26 (2016) 111–119.
[174] H.L. Fan, W.Z. Shen, ACS Sustain. Chem. Eng. 4 (2016) 1328–1337.
[175] Y.S. Yun, K.Y. Park, B. Lee, S.Y. Cho, Y.U. Park, S.J. Hong, B.H. Kim, H. Gwon, H. Kim, S. Lee, Y.W. Park, H.J. Jin, K. Kang, Adv. Mater. 27 (2015) 6914–6921.
[176] Y.N. Singhbabu, S.K. Choudhary, N. Shukla, S. Das, R.K. Sahu, Nanoscale 7 (2015) 6510–6519.
[177] L. Wang, S. Dou, J. Xu, H.K. Liu, S. Wang, J. Ma, S.X. Dou, Chem. Commun. 51 (2015) 11791–11794.

Yang Hou received his Ph.D degree from the School of Environmental Science & Technology of Dalian University of Technology in 2011, and then did 6 years of postdoctoral research in the Department of Chemistry at the University of California, Riverside, Department of Mechanical Engineering, University of Wisconsin–Milwaukee, and Center for Advancing Electronics Dresden, Technische Universität Dresden. He has been a Professor in College of Chemical and Biological Engineering at Zhejiang University since March 2017. His current research focuses on the design and synthesis of low-dimensional nanomaterials for energy and environmental applications.

Yiyong Mai received his Ph.D from Shanghai Jiao Tong University in April 2007 under supervision of Professor Deyue Yan. He joined the group of Professor Adi Eisenberg at McGill University as a Postdoctoral Fellow in September 2008, where he was promoted as a Research Associate in March 2012. He has been a Professor in School of Chemistry and Chemical Engineering at Shanghai Jiao Tong University since March 2013. His present research interest involves synthesis and self-assembly of polymers, as well as functional materials for optoelectronic or energy-related applications.

Xinliang Feng is a full processor and the head of the Chair of Molecular Functional Materials at Technische Universität Dresden since 2014. He received his PhD degree in April 2008 in the Max-Planck Institute for Polymer Research. In December 2007, he was appointed as a group leader at the Max-Planck Institute for Polymer Research, and in 2012, he became a distinguished group leader. His current scientific interests include graphene, synthetic two-dimensional materials, organic conjugated materials, and carbon-rich molecules and materials for electronic and energy-related applications.